C.P. No. 495
(20,470)
A.R.C. Technical Report

C.P. No. 495
(20,470)
A.R.C. Technical Report

MINISTRY OF AVIATION

AERONAUTICAL RESEARCH COUNCIL

CURRENT PAPERS

The Cooling Performance of two Extruded-Type Air-Cooled Turbine Nozzle Blades.

by

R. I. Hodge

LONDON: HER MAJESTY'S STATIONERY OFFICE

1960

SIX SHILLINGS NET

C.P. No.495

U.D.C. No. 621.438-226.3:621-712

Memorandum No. M.311

NATIONAL GAS TURBINE ESTABLISHMENT

July, 1958

The cooling performance of two extruded-type air-cooled turbine nozzle blades

- by -

R. I. Hodge

SUMMARY

A study has been made of the performance of two internally air-cooled turbine nozzle blades made from extruded ventilated sections of similar outside profile. Blade temperatures and coolant pressures were measured in cascade tests over a range of gas conditions and cooling-air proportions.

The effect of the variation in internal geometry is demonstrated in this paper by a comparison between the two profiles, in which the duct hydraulic diameter/blade chord ratios of the ventilating systems were 8.3×10^{-3} and 5.8×10^{-3} respectively, while the duct perimeter/blade chord ratios were roughly equal at 2.9 and 2.8. In this case each cooling system outlet was led into a manifold.

The advantages of manifolding the outlets of the cooling ducts is demonstrated by a comparison of the performances of one of the profiles operated both with and without such a manifold.

The assessment of blade performance at relatively low temperatures demands high accuracy for subsequent conversion to engine operating conditions. Details of the test techniques developed in an endeavour to meet this requirement for high accuracy are included.

CONTENTS

CONTENTS (cont'd)

TABLE

APPENDIX

ILLUSTRATIONS

1.0 Introduction

The acceptance of internally air-cooled blading for use in high temperature gas turbines introduces problems of economic coolant utilisation, and also strain increments within the material due to non-uniform temperature distribution. Much useful information about particular systems can be obtained by measuring the performance of specially instrumented test blades mounted in static cascade. Suitable equipment for this purpose has been installed at the National Gas Turbine Establishment and is described in Reference 1.

An attractive manufacturing method for internally air-cooled turbine blading, embodying extrusion and rolling technique, is currently being developed commercially. By this method suitable blades can be produced having a distribution of ventilating ducts of small hydraulic diameter running spanwise through the component. In cross-section these ducts are of approximately elliptical shape and may lie close to the profile surface, having their major axes parallel to that surface.

Two sample lengths of constant blade profile, differing principally in their internal geometry, have been examined at this Establishment. This Memorandum describes the investigation and the results obtained.

2.0 Scope of the investigation

The two profiles examined, reference numbers Z.1881/13 and Z.1881/18, are illustrated at 5 x full scale in Figures 1 and 2. These test sections were made of Nimonic 80 and 90 respectively. They were tested as follows:-

(i) No. 13, with cooling ducts discharging into a tip clearance space,

(ii) No. 13, with cooling ducts discharging into a tip manifold,

(iii) No. 18, with cooling ducts discharging into a tip manifold.

In this way it was intended that a comparison of the efficacy of the two different internal geometries could be made and secondly that the effect on blade cooling of chordwise static pressure variation across the blade tip could be demonstrated.

In each group of tests the following examination was made:-

(a) Over a range of gas temperatures and throughputs, and coolant flows, readings were taken of (i) spot temperatures on and within the test blade measured by thermocouples, (ii) of the temperatures at points on the neighbouring cascade blade surfaces, and (iii) of coolant pressures at entry to and, where applicable, at exit from the cooling passages.

(b) At particular gas temperatures, throughputs and coolant ratios, the surface temperature patterns were obtained by using temperature-sensitive paint. Apart from the direct interest, this information was also used to provide a relationship between the spot surface temperatures of (a) and the surface mean value of temperature.

(c) A superficial examination of the boundary layer behaviour was made using the lamp-black technique (described in detail in Reference 2).

The investigation (a) above was made, for each group of tests, over the range:-

Gas temperature T_g °K	Reynolds number R_2	Mach number M_2	Coolant ratio W_c/W_g
523	2.3×10^5 to 5.8×10^5	0.25 to 0.85	0.01 to 0.03
773	1.4×10^5 to 3.9×10^5		
1023	10^5 to 3×10^5		

The coolant air entry temperature, T_{c_1}, varied slightly about an average value of 300°K.

2.1 Accuracy requirement

The order of the accuracy to be aimed at in the test programme was deduced from the consideration of the following two hypothetical engine cases:-

(a) Aircraft engine having:-

Gas temperature in blade row, T_g	1250°K
Entry coolant air temperature, T_{c_1}	850°K
Design blade stress	8 tons/in²
Significant change in stress	0.5 tons/in²
Blade material	Nimonic 90

Irrespective of whether rupture in 1000 hr, or 2 per cent strain in 100, 300 or 1000 hr is taken for the design data, the corresponding significant change in blade temperature (equivalent to a change in stress of 0.5 tons/in²) is about 5°C: thus the significant relative temperature variation, $\frac{\Delta T_b}{T_g - T_{c_1}}$, is 0.013.

(b) Industrial engine having:-

Gas temperature in blade row, T_g	1250°K
Entry coolant air temperature, T_{c_1}	450°K
Design blade stress	8 tons/in²
Material design data	Nimonic 90, rupture in 10,000 hr
Significant change in life	2000 hr.

The equivalent significant change in blade temperature is about 7°C in this case, which expressed relatively is 0.009.

From these two cases it was estimated that the desired final test accuracy was ±0.01 on the relative temperature scale.

3.0 Apparatus and method

The tunnel with its instrumentation is described in Reference 1. Figure 3, taken from that reference, shows diagrammatically the layout of the test blade and the neighbouring fixed blades making up the cascade corner. In this series of tests the surface probe was removed.

Surface temperatures measured on the fixed blades are not reported in this Memorandum, but were used in later comparisons between predicted and measured blade temperatures which are the subject of a subsequent statement.

3.1 The instrumented blades

The test blades were assembled from lengths of the ventilated sections brazed into root blocks which accommodated the coolant inlet manifolds. Thermocouples fitted into the profile length were led out through this manifold, which also accommodated the coolant inlet instrumentation. The photograph in Figure 4 gives a view of an assembly, in this case that of the No. 18 profile.

The blade outside design details were slightly different in the two profiles. No. 13 was similar to that of the dummy blades, whereas No. 18, which was designed for another application, varied in minor details from this standard profile:-

		No. 13 and cascade dummy blades	No. 18
Chord	c ft	0.19	0.185
Span	L_s ft	0.371	0.383
Section length	L_p ft	0.408	0.417
Pitch	s ft	0.122	0.122
$\cos^{-1} {}^{o}/_{s}$		65°	58°
Incidence		0°	0°

The internal cooling passage geometry was markedly different in each case: the measured dimensions are given in Table I. Reference 3, which presents a design method for estimating the performance of internally air-cooled blading, shows how the efficacy of the ventilating system may be expressed by a factor

$$Z = \frac{(S_c/c)^{1.2}}{(A_c/c^2)} \qquad \ldots \ldots \ldots \quad (1)$$

where S_c and A_c are the total perimeter and cross-sectional area of the passages. The Z factors for these two profiles are 149 (No. 13) and 213 (No. 18).

The thermocouple instrumentation of the two profiles was somewhat different, that of the second test piece being more ambitious in its coverage than the first. No. 13 had four thermocouples at the midspan position, B, and No. 18 had eleven: the location of these stations is given in Figures 1 and 2. Additionally, No. 18 had thermocouples 1, 3, 5, 7 and 10 at a spanwise position, A, 0.125 ft from the root, and thermocouples 2, 4, 6 and 8 at a third position, C, 0.33 ft from the root surface. The type of instruments used were:-

No. 13 — Pyrotenax 0.062 in. diameter nickel sheathed T1 - T2.

No. 18 — Bristol Aero-Engines Limited
0.032 in. x 0.023 in. nickel sheathed T1 - T2.

In use both types proved sufficiently reliable.

The details in Figures 1 and 2 illustrate the different methods of installation of the surface temperature measuring instruments in the two profiles. In No. 13 the thermocouples were fitted into clearance holes drilled spanwise just below the surface, and were brought out to the surface in relatively large openings: a final brazing operation was used to secure the thermocouple together with a thin cover plate in position. To equip No. 18 spanwise channels were machined in the profile surface and covered with welded-on plates, the thermocouple wires being brought out through small holes in these plates and welded into position. The second method was necessitated by the more congested arrangement of cooling passages in the No. 18 profile, and as subsequent sections will show, is not to be recommended. In both cases the core temperatures were measured by thermocouples which were bundled with Nimonic strips to render them push fits into the holes drilled to the midspan depth.

All thermocouple calibrations were checked to within $\pm 1^{\circ}C$, at the same time, by immersing the particular blade in boiling water, a suction pump drawing the water through the ventilating passages to obviate conduction losses and hence temperature gradients within the material.

Figures 5 and 6 illustrate the coolant measurements. Static pressures are measured in the inlet manifold and, where applicable, in the recess in the tunnel wall forming the outlet manifold. The inlet manifold static pressure was regarded as being equal to the total pressure of the coolant entering the passages, for the flow range covered in the tests. At the outlet, however, the relation between the manifold static pressure and that in the cooling passages is uncertain, as it depends upon the recovery in the very limited space available; this however is a relatively small proportion of the total drop. For measurement of coolant air inlet temperature thermocouples were installed in the cooling-air supply ducts.

3.2 Temperature-sensitive paint tests

"Thermindex" temperature-sensitive paint was used to give visualisation of the surface temperature distribution at particular gas and coolant flows. The test technique followed the methods described in Reference 4. A rod, carrying a number of thermocouples and cooled at one end to give rise to a temperature gradient along its span, was exposed to the gas stream together with, and for the same time as, the test blade. When both blade and rod were sprayed with the paint in an identical fashion, a temperature value for a particular contour could be measured on the calibrating rod and applied to the blade.

In a series of runs to check the reproducibility of the technique it was found that a scatter of $\pm 3^{\circ}C$ appeared in the calibrating rod temperature values for a particular colour change contour. At the blade row conditions at which it was proposed to use this paint change line, such scatter amounted to ±0.01 on the relative scale. This variation appeared to be haphazard and was assumed to be due to differences in application.

The temperature value measured for a particular colour change on the calibrating rod cannot be applied directly to the same contour appearing on the test blade, as is suggested in Reference 4, if the target accuracy of these tests is to be achieved. This is because the drop in temperature through the paint film is substantial, but variable depending upon the local values of heat transfer coefficient and gas/blade temperature difference. For example, the observed differences between the readings of particular blade surface thermocouples with and without a paint film ranged between 3 and $12^{\circ}C$; i.e. at the conditions of the investigation, between 0.01 and 0.04 on the relative scale. It is of interest to note that the calculated thickness of a film of conductivity of the order 10^{-4} CHU/sec·ft which would support such differences with the estimated boundary layer behaviour[2] applied to the profile was everywhere in the order 10^{-3} in.: this agrees with an estimate of the order of thickness of the sprayed coating.

When an appreciable temperature difference is developed through the paint depth, the colour change cannot appear as a perpendicular edge through the film: this may have been the cause of the somewhat indefinite nature of the margin of change from one colour zone to another. This margin was about $\frac{1}{2}$ in. wide on the calibrating rod, but considerably more on some parts of the test blade. By choosing what seemed to be the limit of the colour change on the "cold" side it seemed a reasonable assumption that the calibrating rod temperature was approximately that of the contour at the bottom of the paint depth. The surface temperature would then be this calibrating rod temperature plus the temperature drop through the film. The increment depends, as previously mentioned, upon the heat transfer coefficient and the temperature gradient at the point considered. Such increments were deduced at various points on the test blade profile for the fixed gas flow conditions of the paint tests, by comparing the temperatures measured by individual surface thermocouples at different positions and different metal temperature levels with and without the paint applied.

The test technique may be summarised briefly as follows:-

(a) The gas conditions, Reynolds number and effective temperature, were maintained substantially constant for the paint tests.

(b) The temperature at which the paint changed colour in each particular test was measured by reading the calibrating rod temperature at the position corresponding to the cold side of the colour change margin.

(c) The contour of the cold limit of the colour change margin on the test blade was recorded.

(d) The difference between the blade surface temperatures, with and without a paint coating, was plotted at different profile positions and temperature levels.

(e) The blade contour was corrected by taking increments from the plots (d) for the relevant profile positions at the uncorrected contour temperature (read as blade surface temperature with paint film, see Figure 7). This correction is thus a variable along the contour.

Examples of the plots of the temperature increments are given in Figure 7. These show, for the gas conditions of the Z.1881/13 tests, how such increments are greater near the blade leading edge than at mid-chord on the convex surface, how they increase as the blade surface temperature decreases, and how the effect of paint thickness with the brushed application was observed to be greater than that sprayed. A similar approach with the other test blade, at two gas Reynolds numbers, showed how the increment at the thermocouple station near the L.E. was approximately proportional to $R_2^{0.45}$; the heat transfer coefficients may be expected to vary as $R_2^{0.5}$, but there is a small compensating effect in the variation of $T_g - T_{surface}$, as the increment $T_{surface} - T_{blade}$ increases.

The surface temperature maps of Figures 8, 9 and 10 each result from a number of runs in which the desired Reynolds number and coolant ratio were kept constant, but the gas temperature was varied slightly to cause a particular colour change to appear at different spanwise stations. This to some extent upset the applicability of the increment plots, but this minor inaccuracy was ignored: a better method, had it been available, would have been the control of the coolant temperature. It should be noted that the values appended to the contours are calibrating rod figures, i.e. they are not corrected for the temperature drop through the paint film. This correction is included in the midspan temperature distribution plots given in Figure 11. The examples chosen are Z.1881/13 without tip shroud (brush painted), with tip shroud (sprayed) and Z.1881/18 (sprayed). The differences between the first and second demonstrate the improvement in accuracy achieved as the paint film thickness is reduced: differences between the second and third indicate variations in the boundary layer behaviour on the two profiles.

3.3 Surface thermocouple measurements

The paint tests provided an opportunity for checking that the thermocouples fitted in the blade were unobtrusive, i.e. that their indications were consistent with the temperature which would be measured at the same location in the absence of instrumentation. It was obvious in the case of the No. 18 profile that this was not so (see Figure 10); the colour change contour deviated over the thermocouple channels. The extent of this error is shown up in the additional information in Figure 11. Generally the thermocouples read higher, but in the case of the two T.E. instruments low readings were recorded: it is thought that

this was due to these channels having broken through the division into cooling ducts 1 and 16 (see Figure 2). With the type of instrumentation adopted in the first blade no such errors were observed, and it may be said that that method was unobtrusive.

3.4 Average temperatures from spot readings

Because of the labour involved, the temperature surveys using the indicating paint were limited to a few selected conditions. The surface thermocouples were used to yield average temperatures at the various spanwise stations over the test range described in Section 2.0(a).

This perimeter-average value was obtained from weighted spot readings:-

$$\bar{T}_b = \frac{\omega_1(1) + \omega_2(2) + \omega_3(3) + \ldots\ldots}{\omega_1 + \omega_2 + \omega_3 + \ldots\ldots} \quad \ldots \quad \ldots \quad (2)$$

The weights were assumed to be in linear relationship with the coolant flow proportion, and suitable equations were invented to satisfy the average at the conditions of the paint tests. It was assumed that the selected relations were constant over the entire test range, and this seems probable if serious variations in the boundary layer behaviour are not experienced.

3.5 Inspection of cascade assembly

At the end of the test programme the cascade installation was partially dismantled to permit measurement of the blade pitches and throats. It was found that neither blade was accurately positioned; in the case of the first profile the deviation was not likely to affect materially the boundary layer development, but in the second the discrepancies were of a more serious nature. This blade was found to be slightly warped, which when combined with the positional inaccuracies seemed likely to promote separation from the convex surface over the inboard half of the blade span. The results of these measurements expressed as throat position in terms of total convex surface length, (x/x_s) and trailing edge curvature, in terms of blade pitch divided by the curvature radius, s/e, are as follows:-

		Design	$\frac{1}{4}$ span	$\frac{3}{4}$ span
No. 13	throat	0.48 to 0.54	0.52	0.5 to 0.57
	curvature	0.56	0.58	0.57
No. 18	throat	0.48 to 0.54	0.48 to 0.57	0.49 to 0.52
	curvature	0.49	0.83	0.51

4.0 Test results

In the following sections the test results are presented in comparative pairs, for ease of subsequent discussion. Thus the various measurements are reported in two groups, i.e. the No. 13 profile with and

without tip shroud, and the two profiles both having tip shrouds fitted. A third group contains additional information obtained on the No. 18 profile in its one mode of operation, which is necessary for a discussion of some anomalies observed.

4.1 No. 13 profile, with and without tip shroud

4.1.1 Surface temperature distributions

Referring to the maps on Figures 8 and 9, it will be observed that in the second case, where the tip shroud is fitted, a fan-shaped hot zone originating at the leading edge tip extended into the blade throat over the convex surface. This was obviously a manifestation of the vortex trail generated by the sleeve fitted over the blade tip, which as shown in Figure 5b presented a bluff obstruction upstream of the test blade. It indicates that heat transfer coefficients under such a disturbed flow are relatively great.

The plots of corrected temperature around the profile perimeter, at various spanwise stations, at 1 per cent coolant ratio, given in Figure 12 illustrate the effect of static pressure variation across the blade tip. In the first series this pressure varied from gas inlet to gas outlet static and resulted in a preponderance of the coolant flowing through the trailing edge channels. Presumably as a result of the temperature rise of the coolant in these channels being relatively small the spanwise variation in surface temperature in their vicinity was less than that in the other series. Near the leading edge the cooling channels were relatively starved, and once again the spanwise temperature variation was less than shown in the lower plot. This was particularly true of the sections outboard of the $\frac{1}{4}$ span station; a possible explanation is that the coolant in these channels was fully heated in a short distance resulting in a reduced temperature differential which consequently allowed the blade surface temperature to rise nearly to the effective gas temperature.

On the concave surface of the blade in the second series of tests the temperature contour exhibited a chordwise variation of small amplitude, superimposed on the general pattern. The cooler regions lie between the ventilating channels under this surface, suggesting that the solid metal between the cooling channels acted effectively as fins.

4.1.2 Average surface temperatures

Figure 13 gives midspan perimeter-average temperatures deduced from the thermocouple readings according to the method detailed in Section 3.3. In this Figure best lines have been drawn through the points: the scatter in the first series did not exceed ±0.02, and was generally less than this except in the $W_c/W_g = 0.01$ results; in the second series the scatter did not exceed ±0.01, on the relative temperature scale, in this case also being most marked in the low coolant group.

These temperatures were considerably greater when the blade was operated in the first mode, without a tip shroud, most particularly at low coolant ratios. At the highest ratio the average temperatures were much the same at low Reynolds number, but fitting a coolant outlet manifold displayed an advantage at the upper end of the Reynolds number range. Temperature ratio was more strongly influential in the second series; in the $W_c/W_g = 0.01$ curves from the first series this effect is scarcely discernible. The variation of temperature with Reynolds number was everywhere more marked in the second mode.

4.1.3 Coolant pressure drop

The coolant pressure drop due to friction, heat addition and outlet velocity head loss was taken to be $P_{C_1} - p_{C_2}$. In both cases the static pressure measured in the coolant inlet manifold was taken to be the passage entry total pressure; in the first series of tests, p_{C_2} was assumed to be the mean of the gas inlet and outlet static pressures, i.e. $\frac{p_1 + p_2}{2}$, whereas in the second series it was assumed that the entire outlet velocity head was dissipated in the exit manifold and that p_{C_2} was the static pressure measured there. These pressure drops expressed as a proportion of the blade passage gas velocity head are plotted in Figure 14.

At a gas Reynolds number = 2×10^5, $W_c/W_g = 0.01$ and $T_g/T_{C_1} = 1.75$ the pressure drop coefficients, tip shroud fitted compared with those without tip shroud, are in the ratio 1.1/1. This ratio increases with T_g/T_{C_1} and W_c/W_g until at 3.4 and 0.03 respectively it is 2.6/1. As the absolute loss at given conditions was probably slightly greater in the case with no tip shroud, the comparison suggests that $\frac{p_1 + p_2}{2}$ is not the effective mean coolant outlet pressure. This effective $\overline{p_{C_2}}$ lies between p_1 and p_2 but probably varies with the other parameters. At high Reynolds numbers the first series test pressure drop coefficients changed from the usual negative slope to show an increase with increasing Reynolds number. The maximum Reynolds number readings gave pressure drop coefficients very close to those at the same conditions from the second series.

In both series the effect of temperature ratio appeared to be similar.

4.1.4 Convex side boundary layer condition

Two tests using the lamp-black technique gave results closely similar to those recorded for the copper blade in Reference 2. It seems probable therefore that the development of the boundary layer, in the absence of heat flow between gas and blade, was similar in the two investigations, and therefore the findings of the earlier tests should be applicable in this case.

4.2 Nos. 13 and 18 profiles, both with tip shroud

4.2.1 Surface temperature distributions

A general impression of the surface temperatures can be obtained by comparison of the uncorrected temperature maps in the upper parts of Figures 9 and 10. There is a Reynolds number difference, but not sufficient to affect the general comparison. It will be observed that the "fin" effect on the No. 13 profile is not apparent on the second blade, presumably due to the less localised cooling obtained with the greater number of passages accommodated in the latter. The concave surface patterns are otherwise generally similar, but on the convex side No. 18 exhibits considerably lower temperatures towards the T.E. as is to be expected considering the relative distributions of cooling passages (see Figures 1 and 2).

The advantages of the No. 18 cooling system are more readily seen by reference to Figure 15, where the midspan distributions at similar gas and coolant conditions are compared (the previous No. 13 result for $R_2 = 2.85 \times 10^5$ having been roughly corrected to $R_2 = 2 \times 10^5$). The

gradients on the surface of the No. 18 profile are less severe, and the general level lower than on No. 13. Some over-cooling between $\frac{1}{2}$ and $\frac{3}{4}$ chord on the No. 18 possibly wastes some coolant. The reduction in the temperature of the leading edge is particularly noteworthy.

4.2.2 Average surface temperatures

The Reynolds number range over which the comparison between midspan average surface temperatures can be made on an internal geometry basis is restricted to 10^5 to 2.5×10^5. This is due to the discontinuity in the No. 18 profile results which will be separately discussed in a later section.

Within this range the shape of the curves are generally similar, as shown in Figure 16. At a Reynolds number of 2×10^5, temperature ratio $T_g/T_{c_1} = 2.5$, the relative temperature difference between the two profiles varies between 0.01 to 0.03 over the coolant proportion range 0.01 to 0.03. When the effect of temperature ratio is examined at the same Reynolds number, it is found that the relative degree of cooling $(T_g - T_b)/(T_g - T_{c_1})$ is reduced as temperature ratio increases; the reduction being roughly proportional to $(T_g/T_{c_1})^{-0.25}$ at all coolant flows.

4.2.3 Midspan core temperature

The midspan core temperatures were measured, in the case of No. 13 profile at one central station, and at three positions on the camber line through the No. 18 profile; in this second case the quoted average is the arithmetic mean of the three readings.

The comparison is made in Figure 17. The central regions of the No. 18 profile are considerably cooler than those of the No. 13 profile at the same conditions, and furthermore are better insulated from the surface temperatures, i.e. the difference between average surface and average core temperatures is greater at particular gas and coolant conditions. This insulation effect is separately presented in Figure 18. The two extreme temperature ratios are considered over the coolant flow range, at one gas Reynolds number. While the general relationship with coolant proportion has a similar slope in both cases, the effect of temperature ratio is slightly more marked in the case of the first profile.

A corollary to this insulation effect is of course that proportionately less heat is transferred to the coolant from the core sides of the No. 18 profile cooling ducts than from those of the No. 13 profile for a given coolant temperature at this midspan station.

4.2.4 Coolant pressure drop

The marked difference between the pressure drops necessary to drive given coolant proportions through the two cooling systems is illustrated in Figure 19. Roughly speaking, the flow through the passages of the No. 13 profile was about double that through the No. 18 ducts at particular gas conditions, for a pressure drop equal to one gas outlet velocity head.

The effect of temperature ratio was much the same in both cases, over the test range of Reynolds number and coolant proportion; the average slope of logarithmic plots indicated that the coolant pressure drop coefficient was approximately proportional to $(T_g/T_{c_1})^{-0.2}$ at $W_c/W_g = 0.01$, $(T_g/T_{c_1})^{-0.4}$ at 0.02 and $(T_g/T_{c_1})^{-0.5}$ at 0.03; the effect

of Reynolds numbers on these approximations was negligible. When power approximations of the above nature are accepted, the pressure loss coefficients are seen to be in the ratio, No. 16 to No. 13, of about 2.5/1, at particular gas and coolant conditions. This is roughly the same as the square of the ratio of total passage cross-section areas in No. 13 and No. 18 profiles.

4.3 No. 18 profile

A discontinuity is apparent in the plots of average surface temperature versus Reynolds number (Figure 16b). It occurs at about $R_2 = 3 \times 10^5$, and results in blade temperatures everywhere higher than would occur were the trends of the low Reynolds number results to continue, as indeed they do in the case of the other profile. Insufficient data was obtained to determine the shape of the curves above $R_2 = 4 \times 10^5$, and the accuracy target of 0.01 on the relative temperature scale had to be abandoned. The influence of the temperature ratio is thought to be less than at the low end of the range, but this opinion is based on a very limited number of observations. Similar discontinuities but of different magnitudes were also observed in the plots of core temperature (Figure 17b) and of surface temperatures at stations other than the midspan.

4.3.1 Surface temperature distribution

An additional set of paint colour change contours was obtained at a Reynolds number of 4.5×10^5, so that the detail nature of this discontinuity could be observed. This pattern is presented in Figure 10b. It is apparent that the concave surface behaviour is little different, but that the last part of the convex surface is relatively hotter at the higher flow.

The perimeter distribution at three spanwise stations for Reynolds numbers of 2 and 4.5×10^5 (Figure 20) shows this effect more clearly.

4.3.2 Convex side boundary layer behaviour

The change in the convex side temperature pattern described in the previous section suggested that the nature of the boundary layer over this surface was markedly different at the two extremes of the flow range. A lamp-black visualisation examination was therefore made over this surface.

Lamp-black records were obtained over the Reynolds number range 3.8×10^5 to 7.5×10^5, at a gas temperature = 300°K. These fell into four main categories as far as the convex side is concerned, as shown in Figure 21:-

(1) Undisturbed deposit over the entire surface up to $R_2 = 4 \times 10^5$. This indicated a low level of turbulence in the main stream but yielded no information about laminar separation.

(2) The deposit slightly abraded from L.E. to $x/x_s = 0.8$: this was the usual appearance under a laminar boundary layer in high speed flow. At about $x/x_s = 0.8$ however the deposit was unmarked: this state extended to near the T.E. where, outboard of midspan, the blade metal was exposed. This

was interpreted as indicating laminar separation followed locally by transition to turbulence sufficiently near the blade surface to affect it. This type of plot was recorded up to $R_2 = 6.7 \times 10^5$.

(3) In the range 7.1×10^5 to 7.4×10^5 marked differences were observed between root half and tip half. Inboard of midspan the record was similar to that described in (2) above except that the demarcation occurred earlier. Outboard of midspan the deposit was removed from $x/x_s = 0.5$ to trailing edge. It is possible that the boundary layer was separated from this part of the surface over the root half and was attached, but turbulent elsewhere. The Reynolds number range of this mode is short, and two records as described in (4) below were obtained within this range, indicating that this was not a stable mode.

(4) At the upper limit of Reynolds number a fourth type of trace was discovered: again there are differences on either side of midspan. Inboard the logical interpretation of Figure 21c is transition at about $x/x_s = 0.45$, separation at 0.6: outboard it is transition at about 0.5, separation at 0.65 and finally re-attachment at 0.9.

These records were obtained without combustion at low levels of mainstream turbulence. Reference 2 contains a survey of the cascade turbulence levels, and also a tentative description of the interaction of turbulence with the other boundary layer parameters controlling separation and transition. This latter survey demonstrated, for example, that a given transition observed at $R_2 = 7.4 \times 10^5$ at the level of these tests might be expected at $R_2 = 3.6 \times 10^5$ with the turbulence obtaining when the combustion chambers are operated. Thus the changes demonstrated in the lamp-black tests were probably effective at the flows at which the blade temperature discontinuities were observed.

5.0 Discussion

5.1 The effect of manifolding the cooling duct outlets

The tests on the Z.1081/13 profile demonstrate clearly the effects of the static pressure variation across the blade chord on the coolant distribution. The concentration of the coolant flow in the T.E. passages results in these regions being reduced to relatively low temperature levels, but permits the L.E. to rise to very near the effective gas temperature. Although the average surface temperature and coolant pressure drop versus coolant flow relations are only affected to a minor degree by variations in flow distribution, the utility of the system is seriously reduced when large variations in temperature occur over the blade chord, as in the former case.

Manifolding the outlet appears to correct the tendency. An alternative solution might be the changing of the location of the passages but an examination of the profile drawing shows that little could be done in this direction, without introducing serious local gradients between passages in the T.E. half of the section. Metering orifices in the T.E. passages would serve to correct the tendency, but only at the cost of increased pressure drop.

5.2 Contrast between two geometries

The decrease in the hydraulic diameter of the cooling passages has only a minor (but significant) effect on the average temperatures at given gas and coolant flow conditions. Increasing the dispersion of the passages and the cooling heat transfer coefficients serves to insulate the core of the blade from the surface, which means that a large proportion of the internal surfacing is at a relatively low temperature and thus contributes less to the overall heat flow. This contrary development reduces the effectiveness of the ventilating passages as far as surface temperature is concerned. On the other hand, if the temperature gradients can be accommodated, the cooler core might take higher loadings.

The improvements are paid for by marked increases in the coolant pressure drop. If coolant utilisation is not the controlling factor, profiles with large ventilating hydraulic diameters would be used. In this comparison for example, at $R_2 = 2 \times 10^5$, $T_g/T_{c_1} = 2.5$ and $\frac{P_{c_1} - p_{c_2}}{\frac{1}{2}\rho_g V_g^2} = 1$, the No. 13 profile would have a midspan average temperature (relative) of about 0.56, and the core would run at about 0.5; the No. 18 profile would have temperatures of 0.69 and 0.65 respectively. The coolant flows permitted would, however, be about 2.6 per cent in the first case and half that in the second.

A noteworthy effect, due principally to modifications in the external geometry of the second profile, is illustrated in the temperature distributions about the L.E. in Figure 15. The peak is sharper in the case of the No. 13 profile, and this is thought to be due to the leading edge radius/blade chord ratio rather than to improvement in the cooling. The values of the ratio are 0.030 and 0.045 respectively, and Reference 3 points out how heat transfer coefficients at the stagnation point may be reduced by increases in the leading edge radius.

5.3 Dependence upon boundary layer behaviour

Major increases in local temperature were experienced when the boundary layer separated from the blade convex surface: for example, at $x/x_s = 0.8$ at spanwise station A, the relative temperature increased from 0.66 to 0.75, as shown in Figure 20. The effect on the average surface temperature at this station, for coolant flow proportion = 0.01, was about 0.02 on the relative scale. The subject of separated flows is discussed in Reference 2, where it is shown that local heat transfer coefficients are very high under separated flows, at some positions some 40 per cent greater than those under attached turbulent boundary layers.

Cooled turbine blades are thus doubly vulnerable to flow separation, on the score of both aerodynamic performance losses and heat transfer.

6.0 Conclusions

The description of the investigation includes details of the instrumentation and of the test techniques adopted in the attempt to record blade perimeter-average surface temperatures to an accuracy of ±0.01 on the relative scale.

In this way a study was made of a ventilated profile operating in two modes, with and without a manifold about the cooling passage

outlets. The superiority of the manifolded mode is demonstrated.

The relative merits of two distributions of internal passages is illustrated in performance comparisons between the two profiles: in one the ratio of the hydraulic diameter of the complete cooling system to the blade chord was 8.3×10^{-3}, in the other 5.8×10^{-3}: the cooling perimeters were approximately equal in the two cases. For a given cooling flow the one having the smaller passage ratio was marginally better cooled at the surface, but core temperatures were materially reduced. The pressure loss was about 2.5 times that experienced in the larger passages.

The leading edge radius is an important design feature in cooled blades, in that stagnation point heat transfer coefficients are large about sharp edges. The effect of increasing this radius by 50 per cent is shown in the midspan surface temperature distributions in Figure 15.

The second blade profile was slightly warped in manufacture: this led to separation of the boundary layer over part of the convex surface above a certain gas Reynolds number. The effect of this development was a major increase in local surface temperatures.

ACKNOWLEDGEMENT

The author wishes to acknowledge his appreciation of the valuable assistance rendered by Messrs. Henry Wiggin & Co., in particular Mr. C. C. Horne, in producing the extrusion from which the test blades were constructed.

REFERENCES

No.	Author(s)	Title, etc.
1	R. I. Hodge	A turbine nozzle cascade for cooling studies. Part I The measurement of mean Nusselt numbers at the blade surface. C.P.492. May, 1958.
2	R. I. Hodge	A turbine nozzle cascade for cooling studies. Part II Comparison between measured and predicted mean Nusselt numbers at the blade surface. C.P.493. May, 1958.
3	D. G. Ainley	Internal air-cooling for turbine blades. A general design survey. A.R.C. R. & M. No. 3013, 1957.
4	A. G. Smith R. D. Pearson	The cooled gas turbine. Proc. I. Mech. E., Vol. 163, 1950.
5	D. G. Ainley G. C. R. Mathieson	An examination of the flow and pressure losses in blade rows of axial flow turbines. A.R.C. R. & M. No. 2891, March, 1951.

TABLE I

The dimensions of the internal ventilating ducts

(a) Profile Z.1881/13

Passage No.	Area $ft^2 \times 10^{-5}$	Perimeter ft $\times 10^{-2}$
1	8.14	4.52
2	7.52	4.17
3	7.59	4.25
4	7.79	4.32
5	8.41	4.92
6	8.20	5.64
7	6.84	5.92
8	8.14	5.97
9	8.54	5.42
10	8.34	5.20
11	7.79	4.72
TOTAL	$A_c = 87.4 \times 10^{-5}$	$S_c = 55.10 \times 10^{-2}$

(b) Profile Z.1881/18

Passage No.	Area $ft^2 \times 10^{-5}$	Perimeter ft $\times 10^{-2}$
1	1.88	2.75
2	3.06	3.67
3	3.40	2.92
4	3.40	2.83
5	3.06	2.75
6	3.40	2.75
7	3.96	3.08
8	3.96	2.75
9	3.96	3.00
10	3.06	3.17
11	4.17	3.33
12	3.06	3.33
13	3.40	3.42
14	3.82	3.92
15	3.82	3.83
16	3.82	4.25
TOTAL	$A_c = 55.21 \times 10^{-5}$	$S_c = 51.75 \times 10^{-2}$

APPENDIX I

Notation

A_c cooling duct total cross-sectional area

c blade chord

c_p gas specific heat at constant pressure

e radius of convex side curvature between throat and trailing edge

L_p section length

L_s span

M Mach number in gas stream

$\overline{M}$ average Mach number around profile

σ blade throat opening

P total pressure

p static pressure

R_2 blade outlet Reynolds number $= \dfrac{W_g \cdot c}{s \cdot L_s \cdot \cos \sigma/s \cdot \mu_g}$

s blade pitch

S_c cooling duct total perimeter

T total temperature

T_b blade point surface temperature

$\overline{T_b}$ perimeter-average surface temperature at a given spanwise station

T_{bc} blade camber line point temperature

T_g gas effective temperature $= T_1 \left[1 - 0.15 \left\{ \dfrac{\frac{\gamma - 1}{2} \overline{M}^2}{1 + \frac{\gamma - 1}{2} \overline{M}^2} \right\} \right]$

V_{g_2}	gas velocity in blade throat
W_c	coolant flow rate in test blade
W_g	gas flow rate per blade passage
x	blade perimeter length measured from L.E.
x_s	convex surface length
$\omega_1, \omega_2, \omega_3$	weighting factors in midspan perimeter-average temperature equation
μ_g	absolute viscosity of gas measured at T_g
ρ_g	density of gas measured at p_2 and T_g

Positional suffices

1	blade passage entry
2	blade throat
m	midspan
c_1	cooling entry manifold
c_2	cooling passage outlet

NOTE: T expressed as a relative temperature is $\frac{T - T_{c1}}{T_g - T_{c1}}$

FIG. 1.

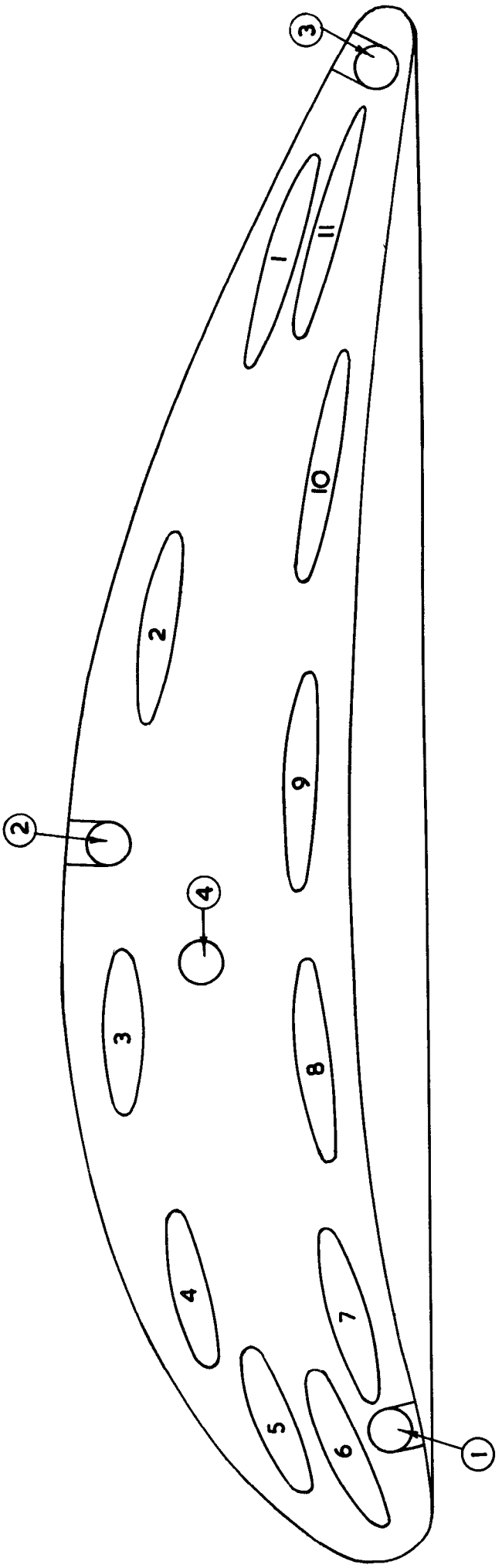

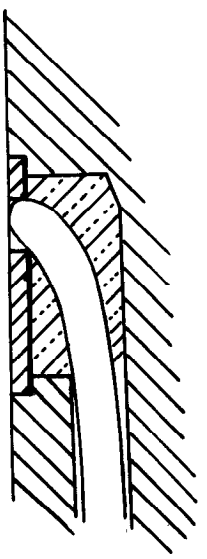

DETAIL SHOWING THERMOCOUPLE IN POSITION

Z 1881/13
INSTRUMENTED PROFILE

FIG. 2.

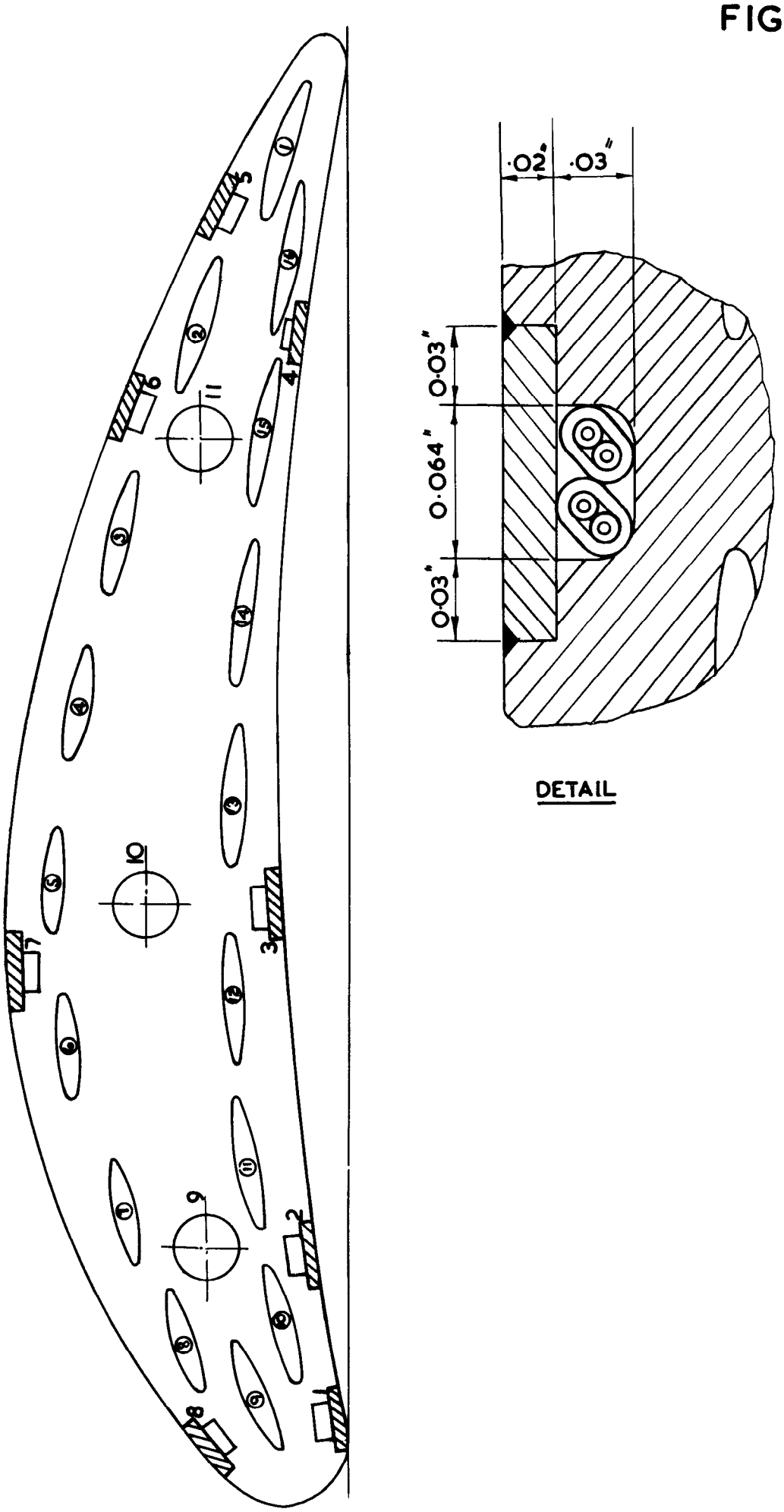

Z 1881/18
INSTRUMENTED PROFILE

FIG. 3.

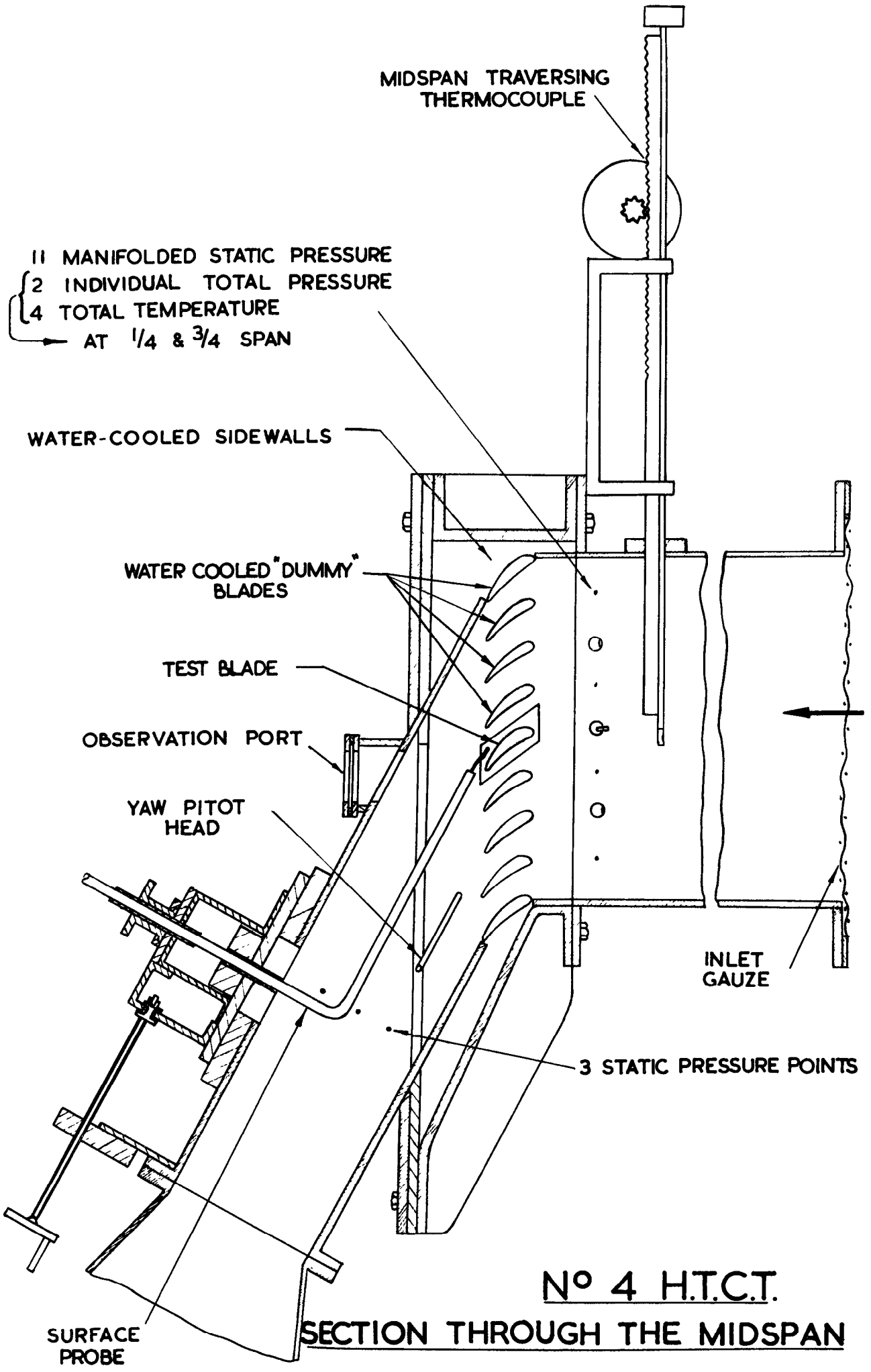

Nº 4 H.T.C.T.

SECTION THROUGH THE MIDSPAN

FIG. 4.

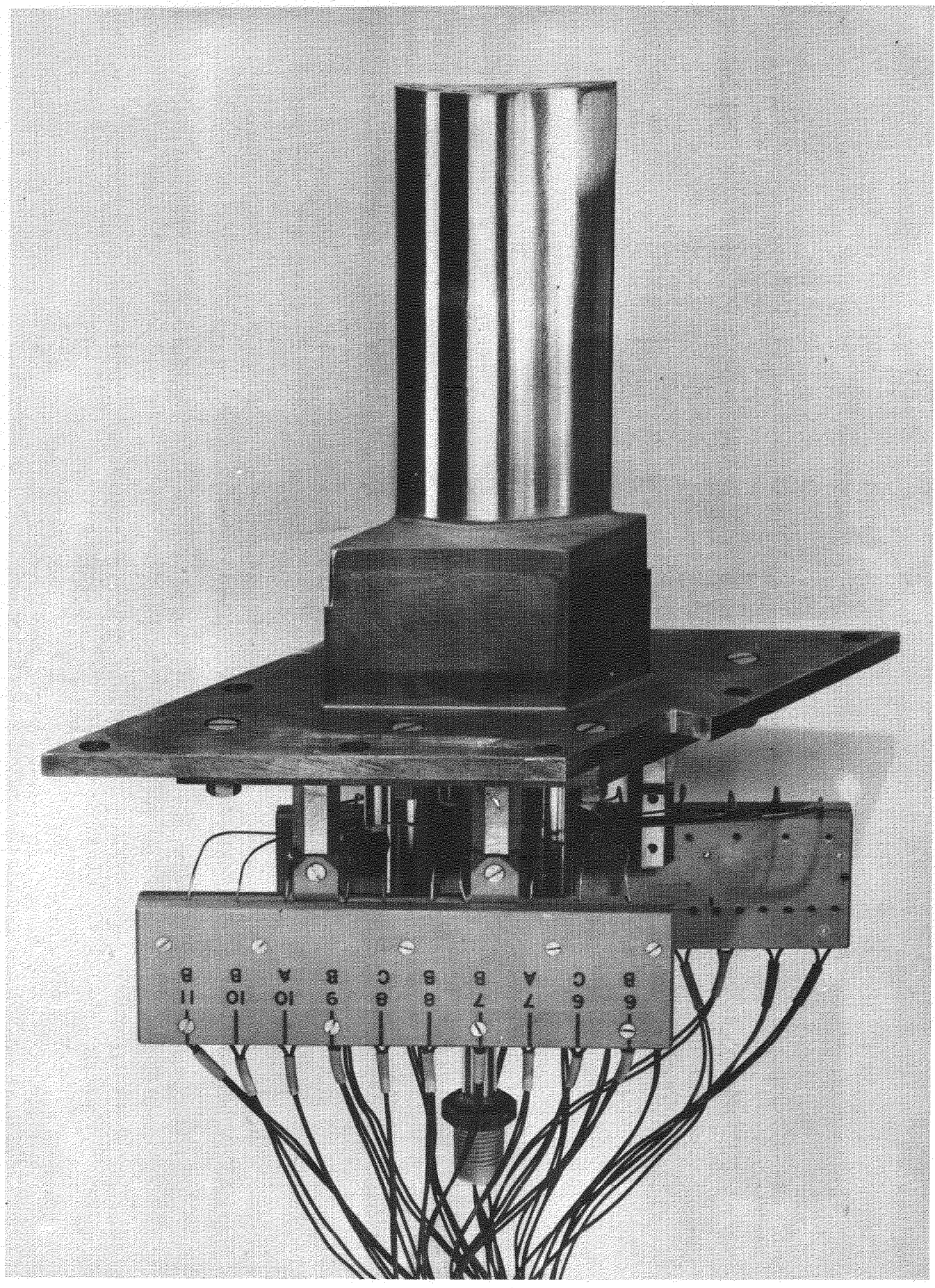

FIG. 5.

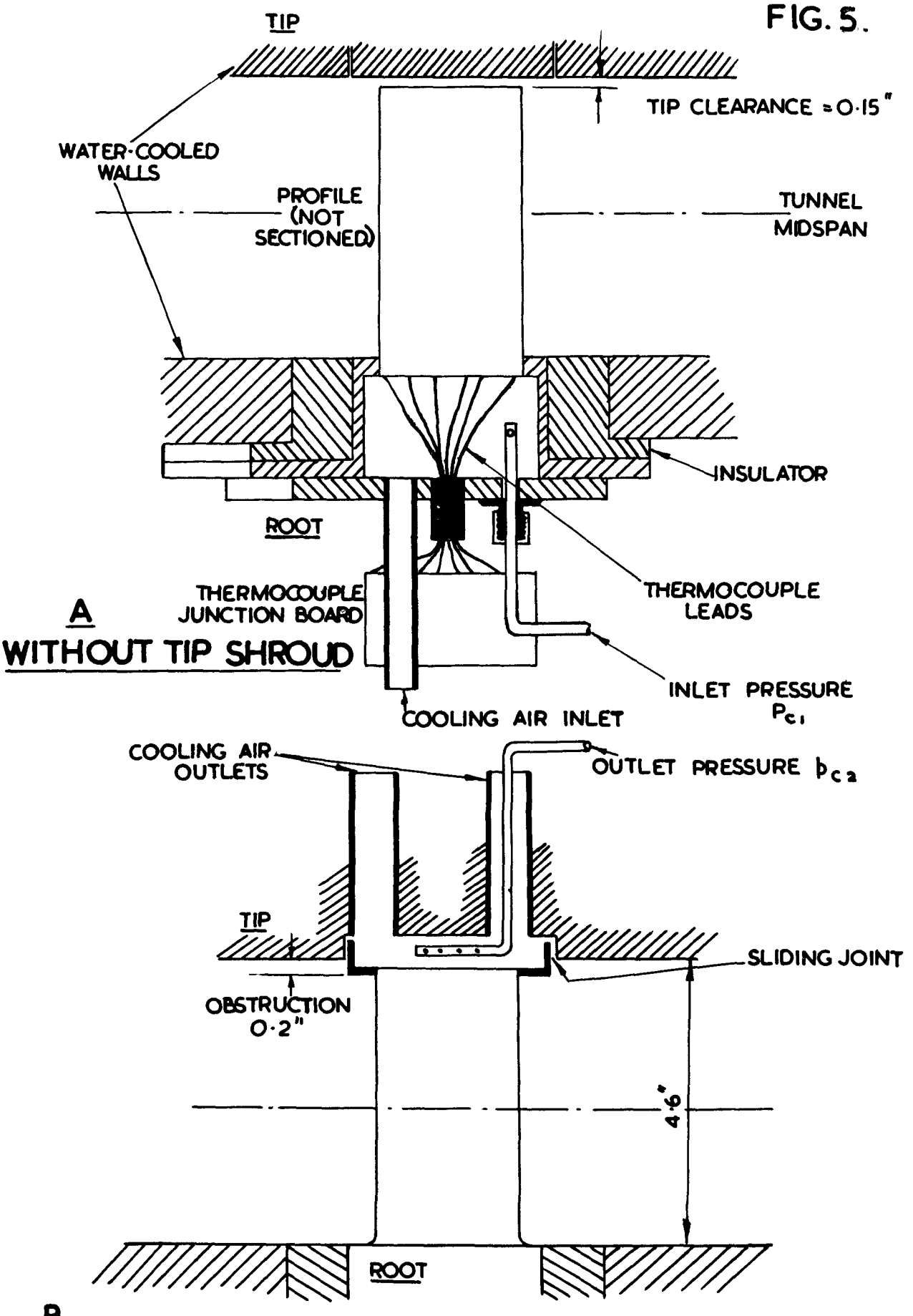

Z 1881/13

TUNNEL INSTALLATION

FIG. 6.

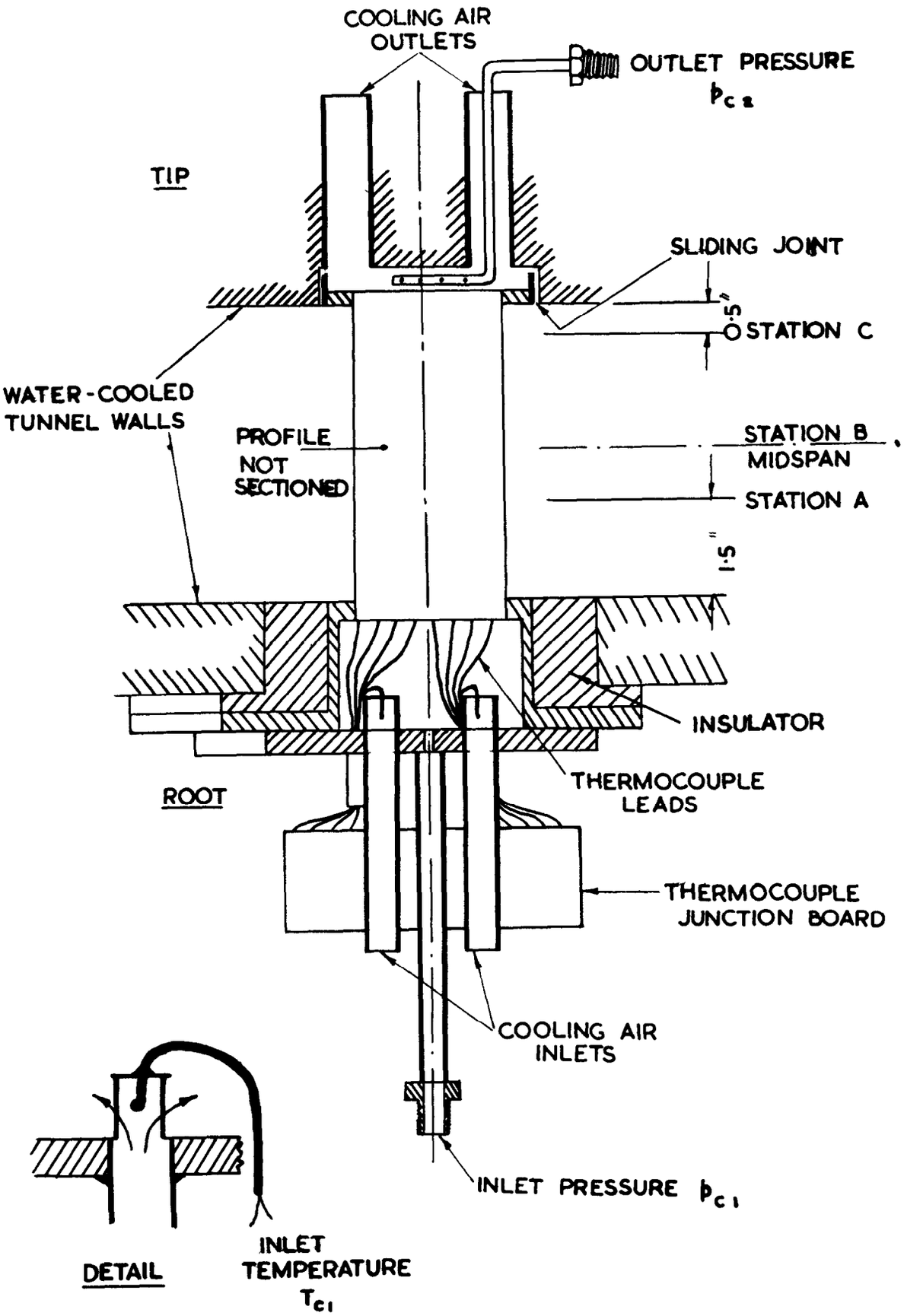

Z 1881/18

TUNNEL INSTALLATION

FIG. 7.

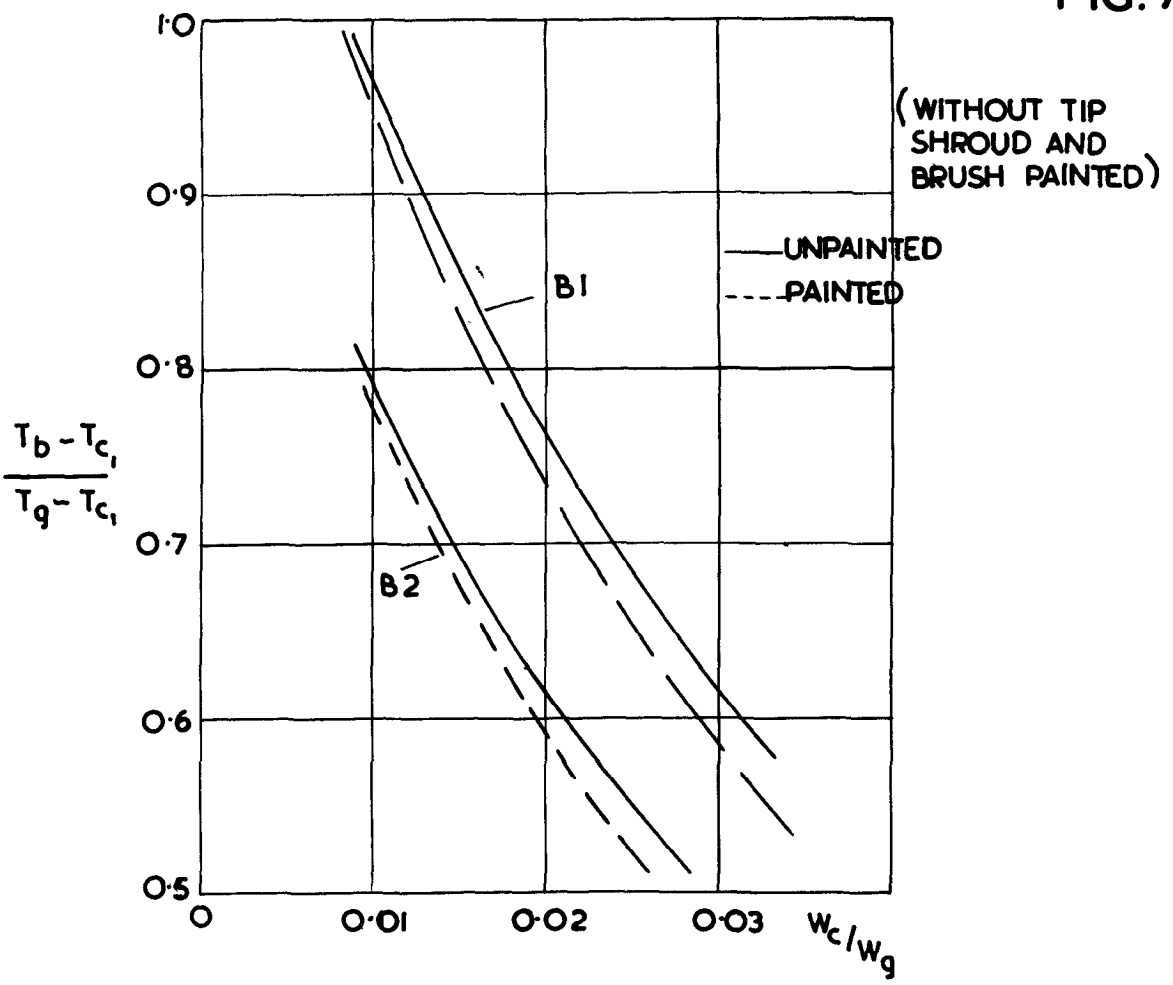

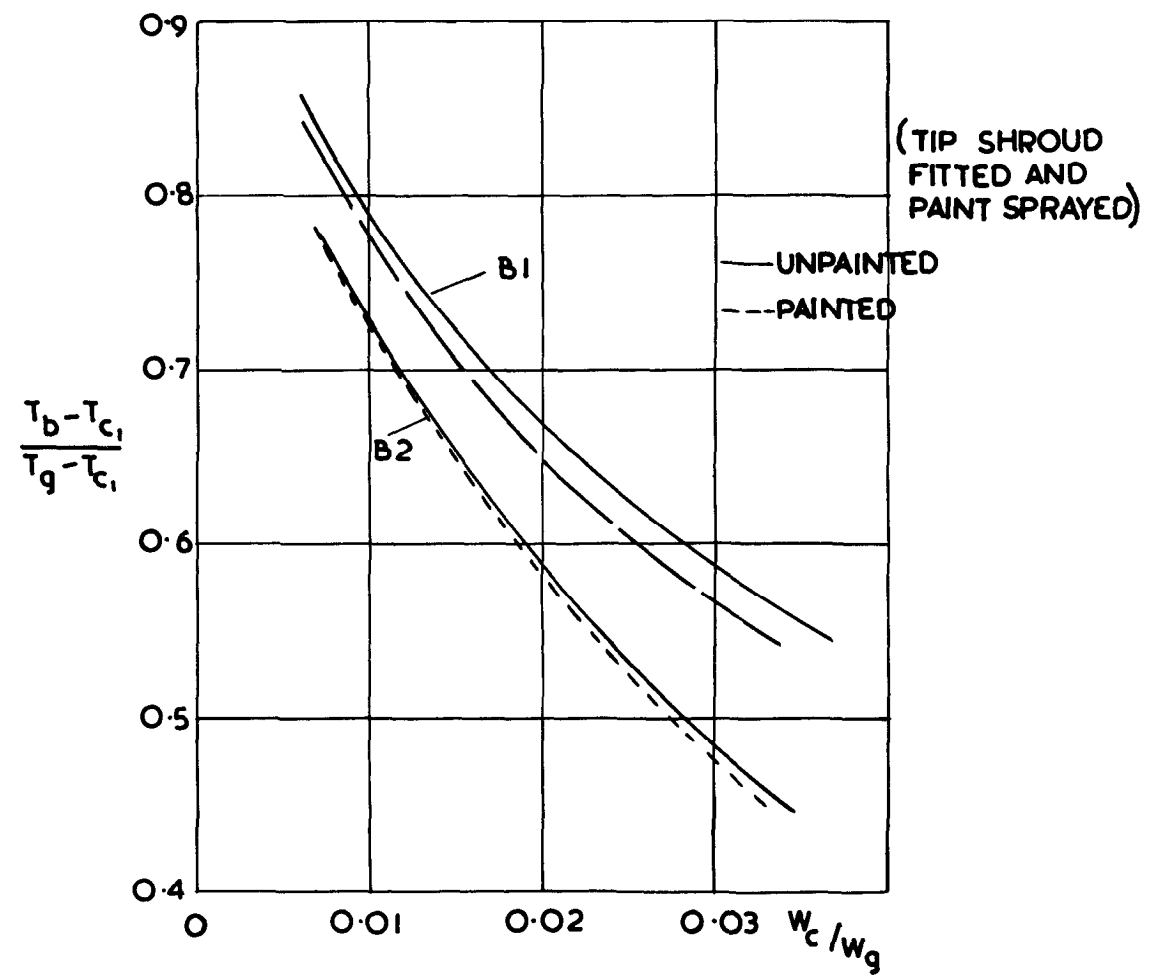

Z 1881/13

THERMINDEX PAINT TEMPERATURE CORRECTION

FIG.8.

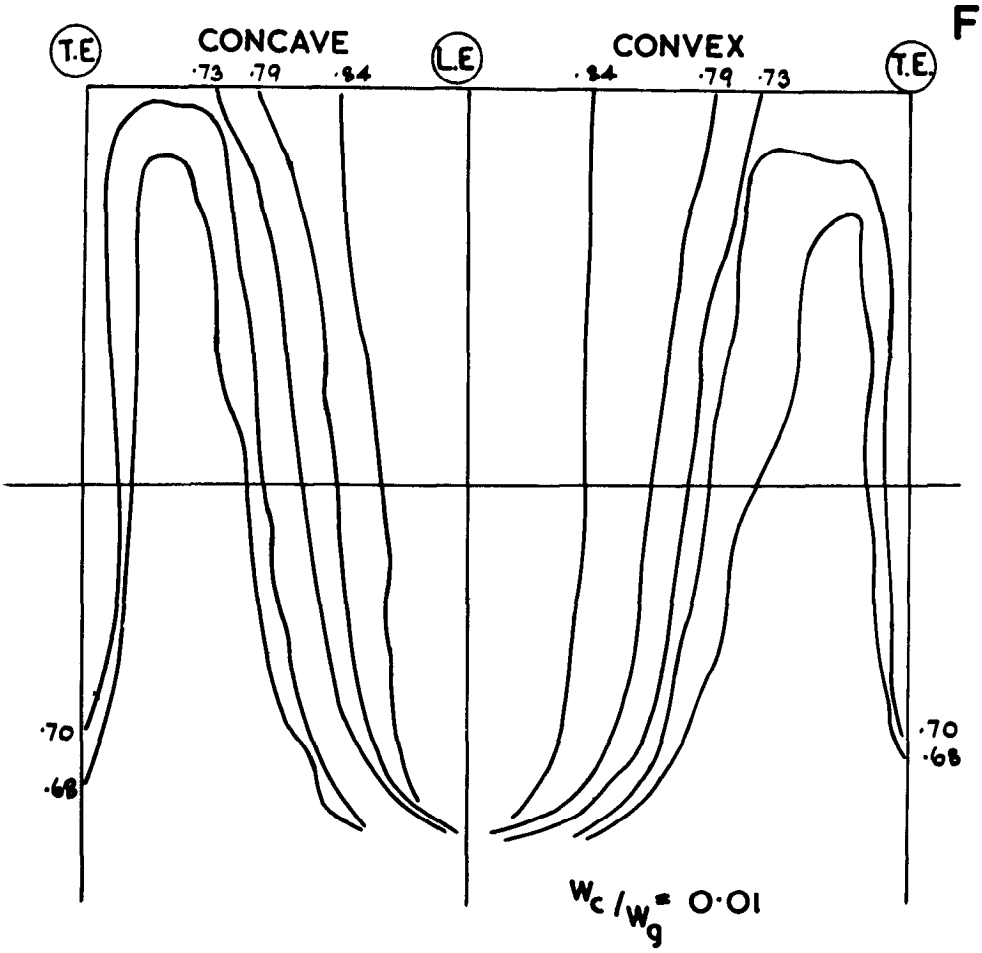

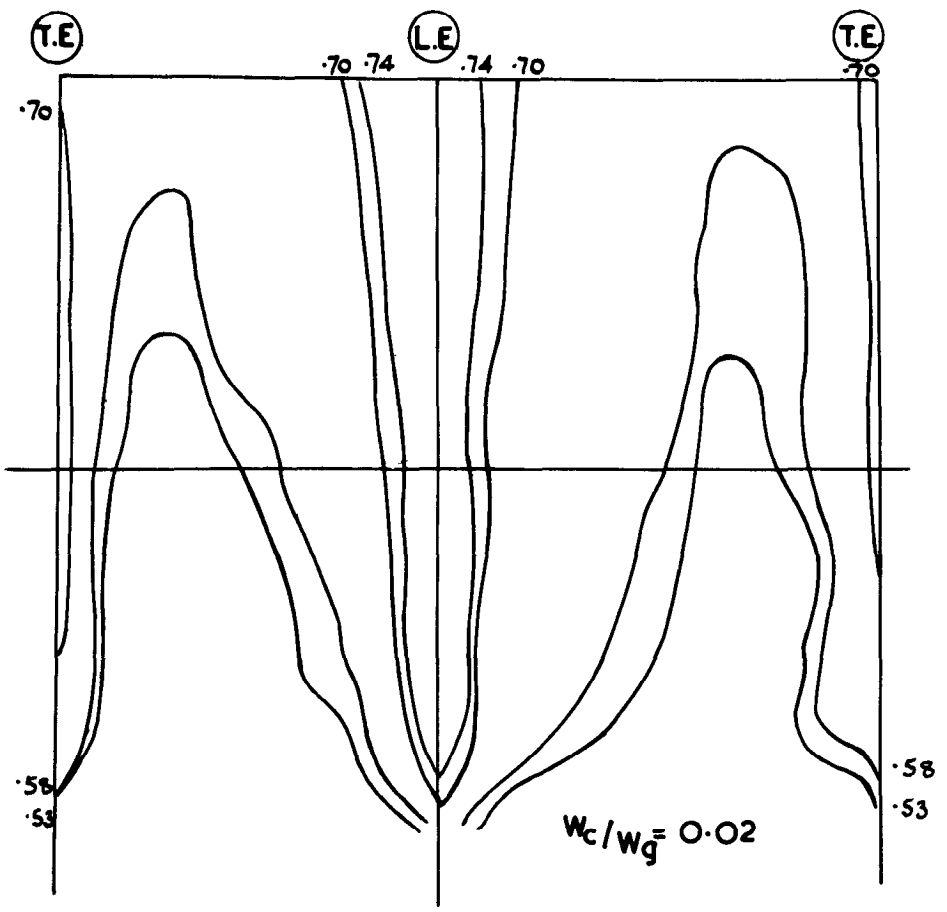

$R_2 = 2.8 \times 10^5$ $T_g/T_{C_1} \simeq 1.9$

Z 1881/13

PAINT TEMPERATURE CONTOURS

WITHOUT TIP SHROUD

FIG. 9.

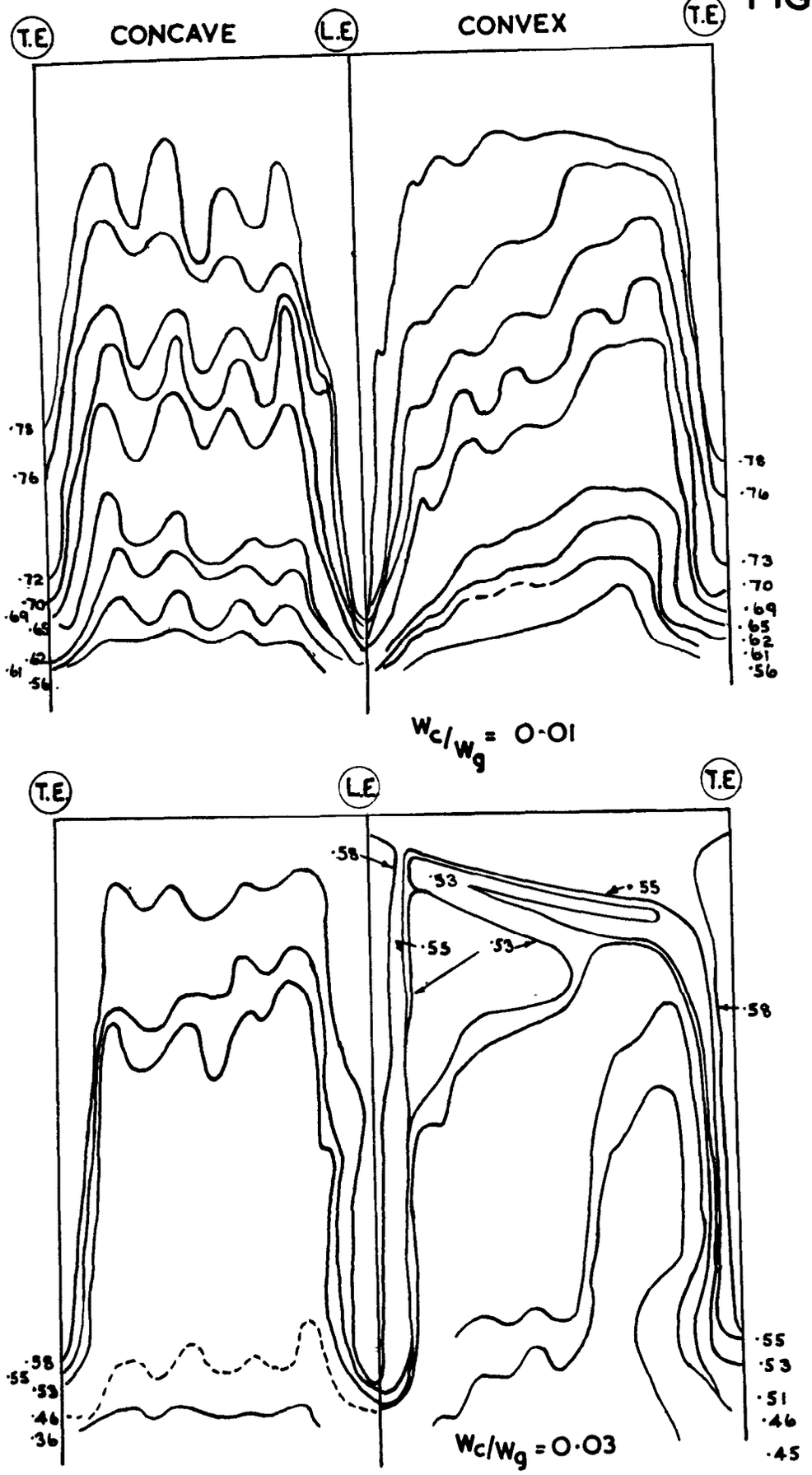

$R_2 = 2{\cdot}85 \times 10^5$ $T_g/T_{c_1} \simeq 2$

Z 1881/13

PAINT TEMPERATURE CONTOURS WITH TIP SHROUD

FIG.10

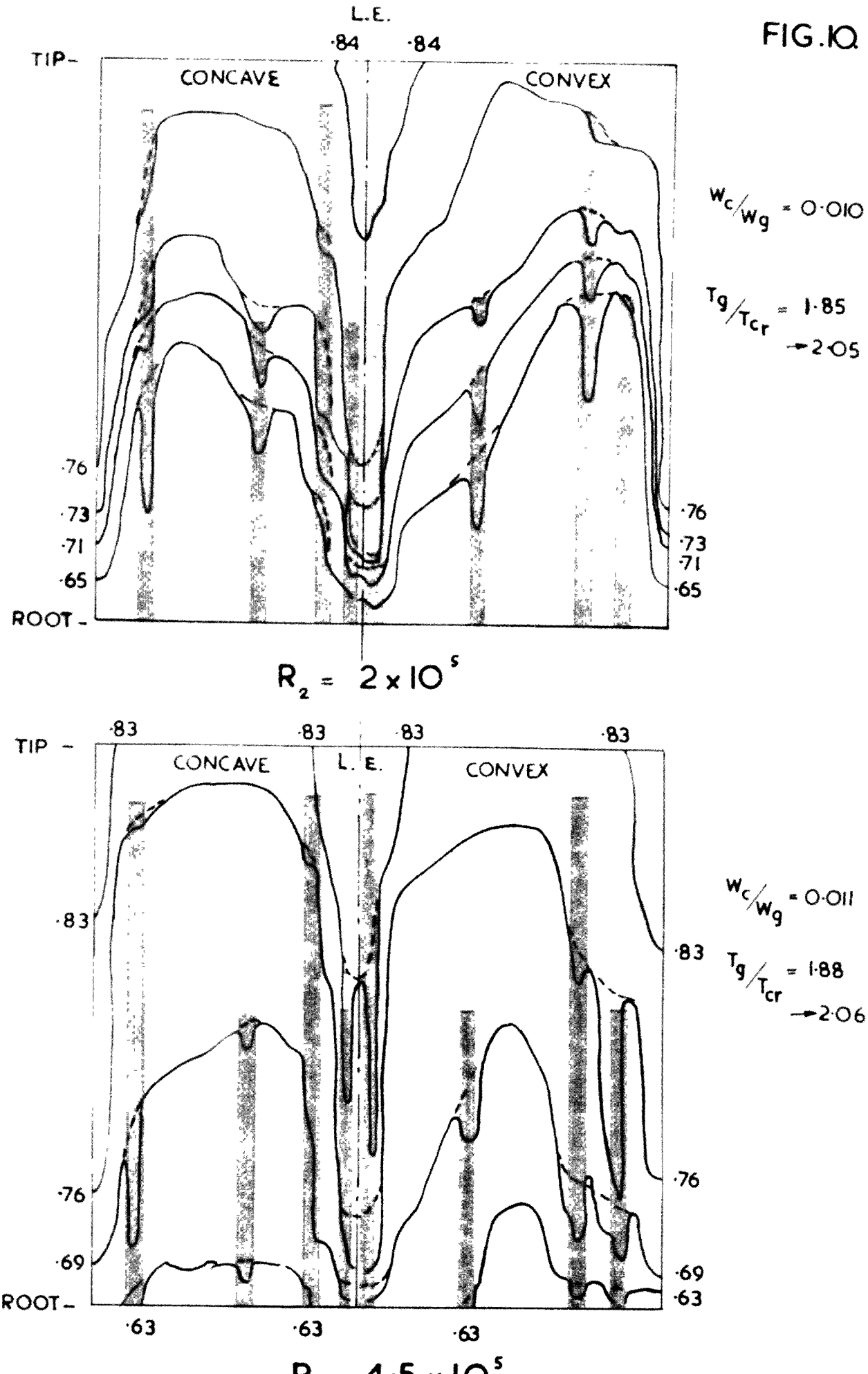

Z 1881/18

PAINT TEMPERATURE CONTOURS

FIG. 11.

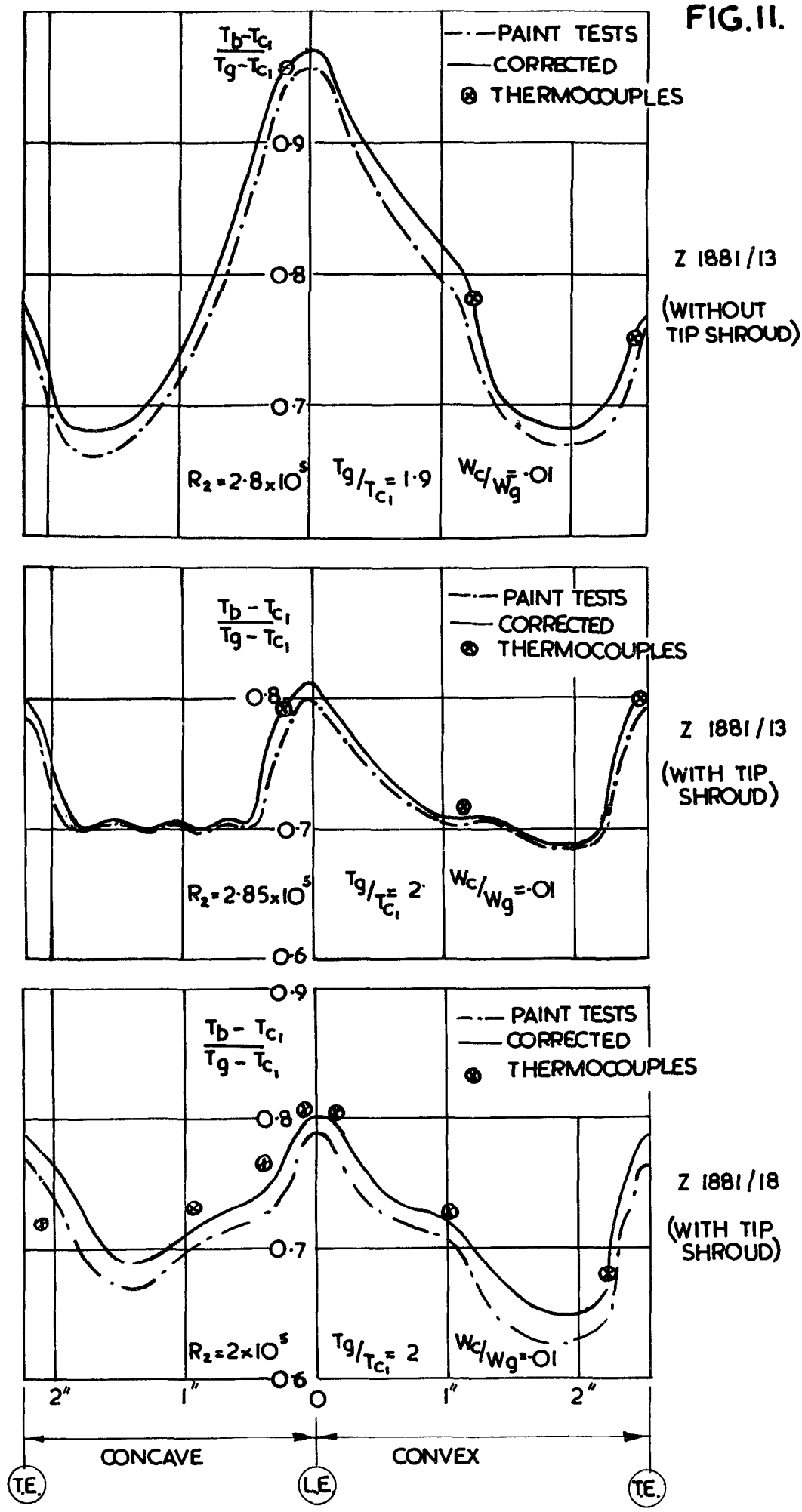

CORRECTED TEMPERATURE DISTRIBUTIONS AT MIDSPAN

FIG.12.

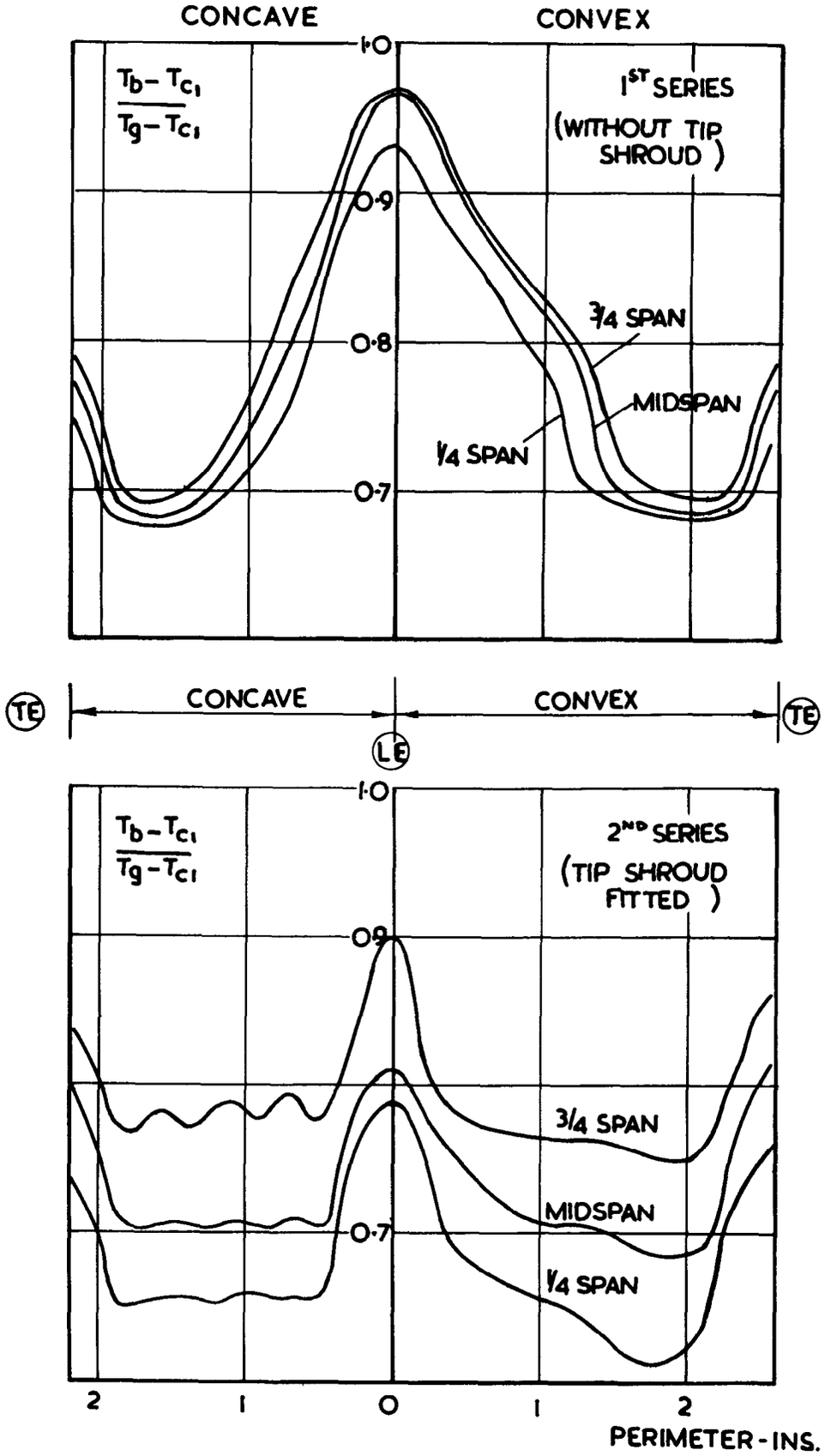

$R_2 = 2{\cdot}85 \times 10^5$

$T_g / T_{c_1} \simeq 2$

Z 1881/13

TEMPERATURE DISTRIBUTIONS AT $W_c/W_g = {\cdot}01$

FIG. 13.

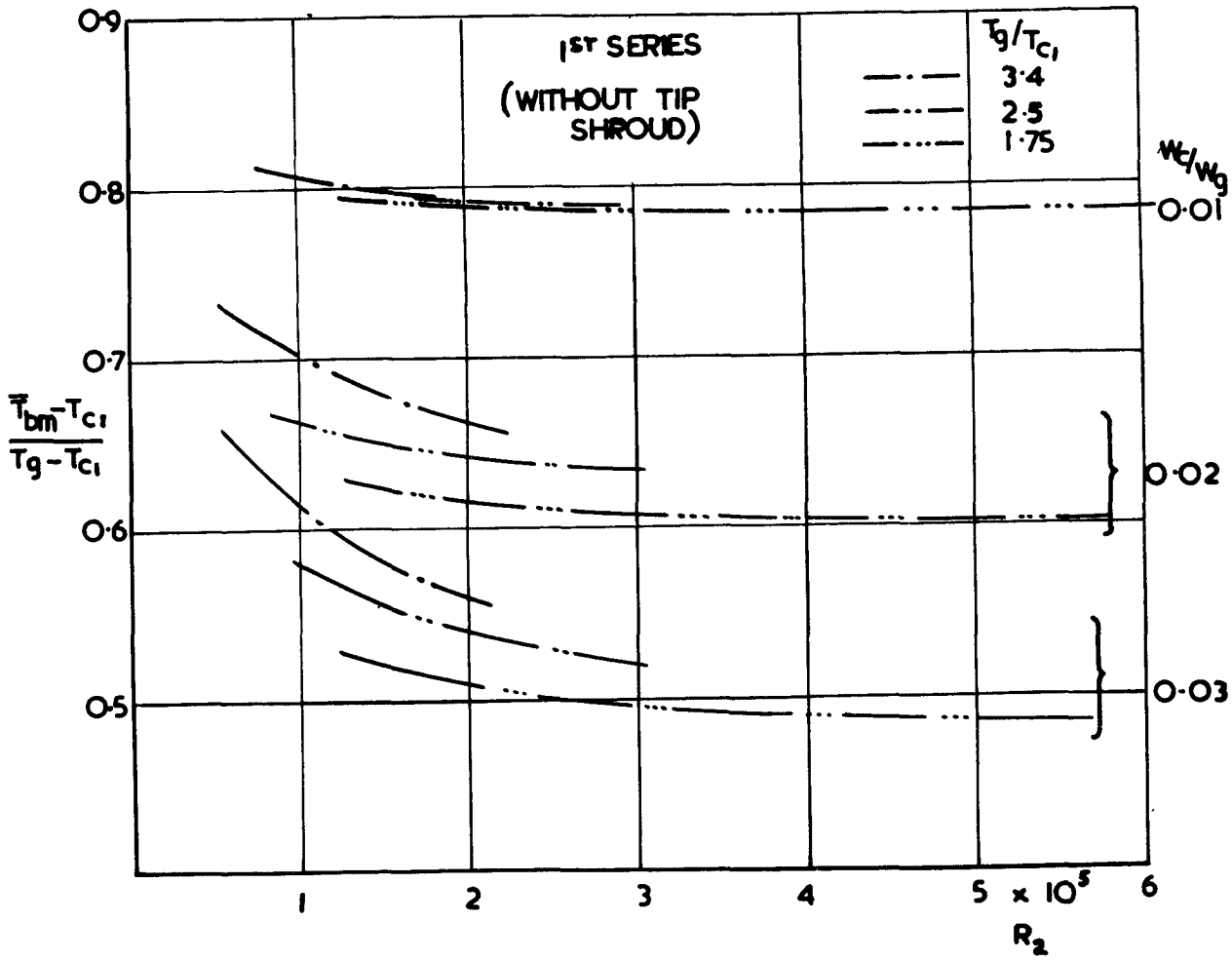

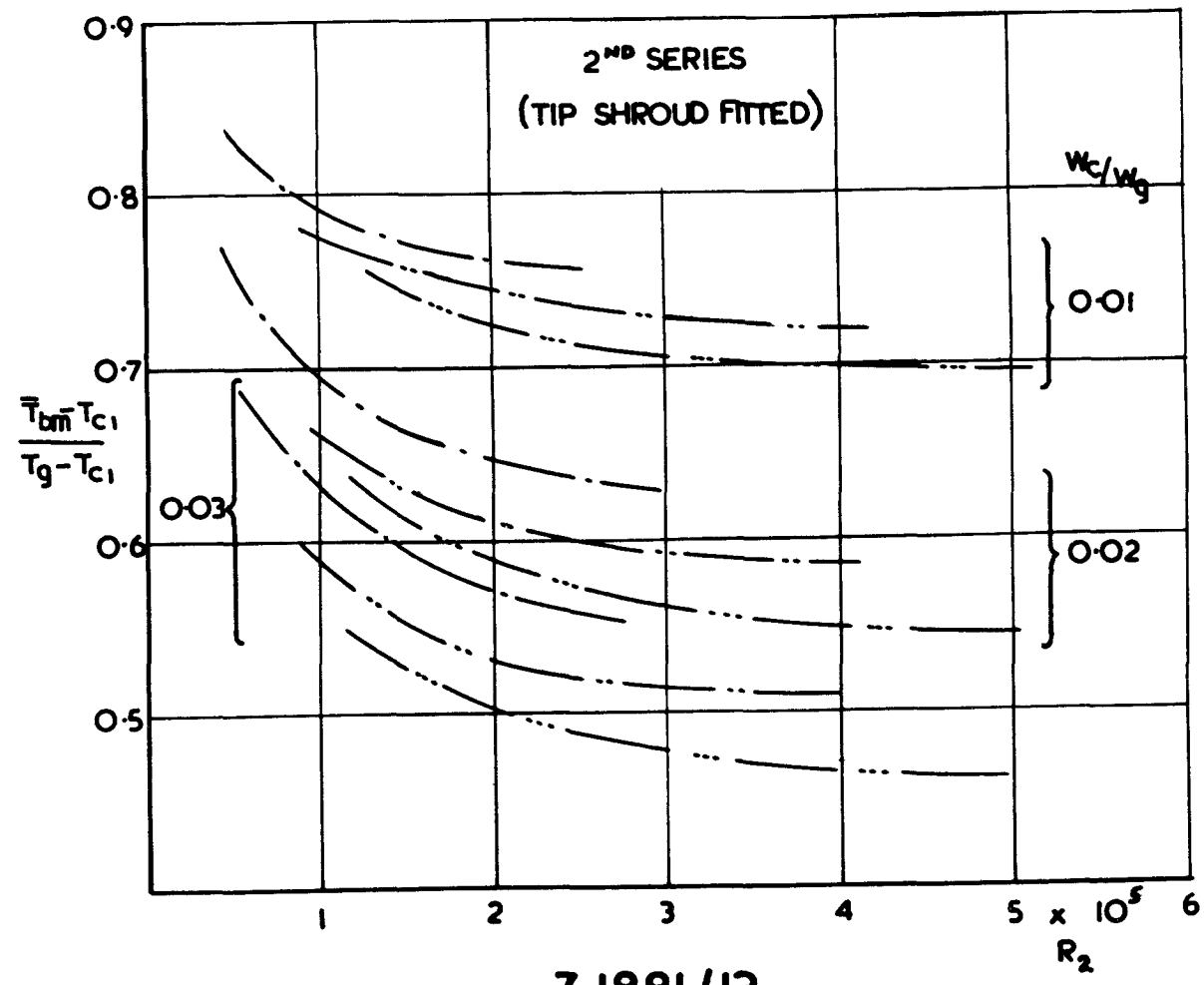

Z 1881/13

AVERAGE PROFILE SURFACE TEMPERATURE AT MIDSPAN

FIG. 14.

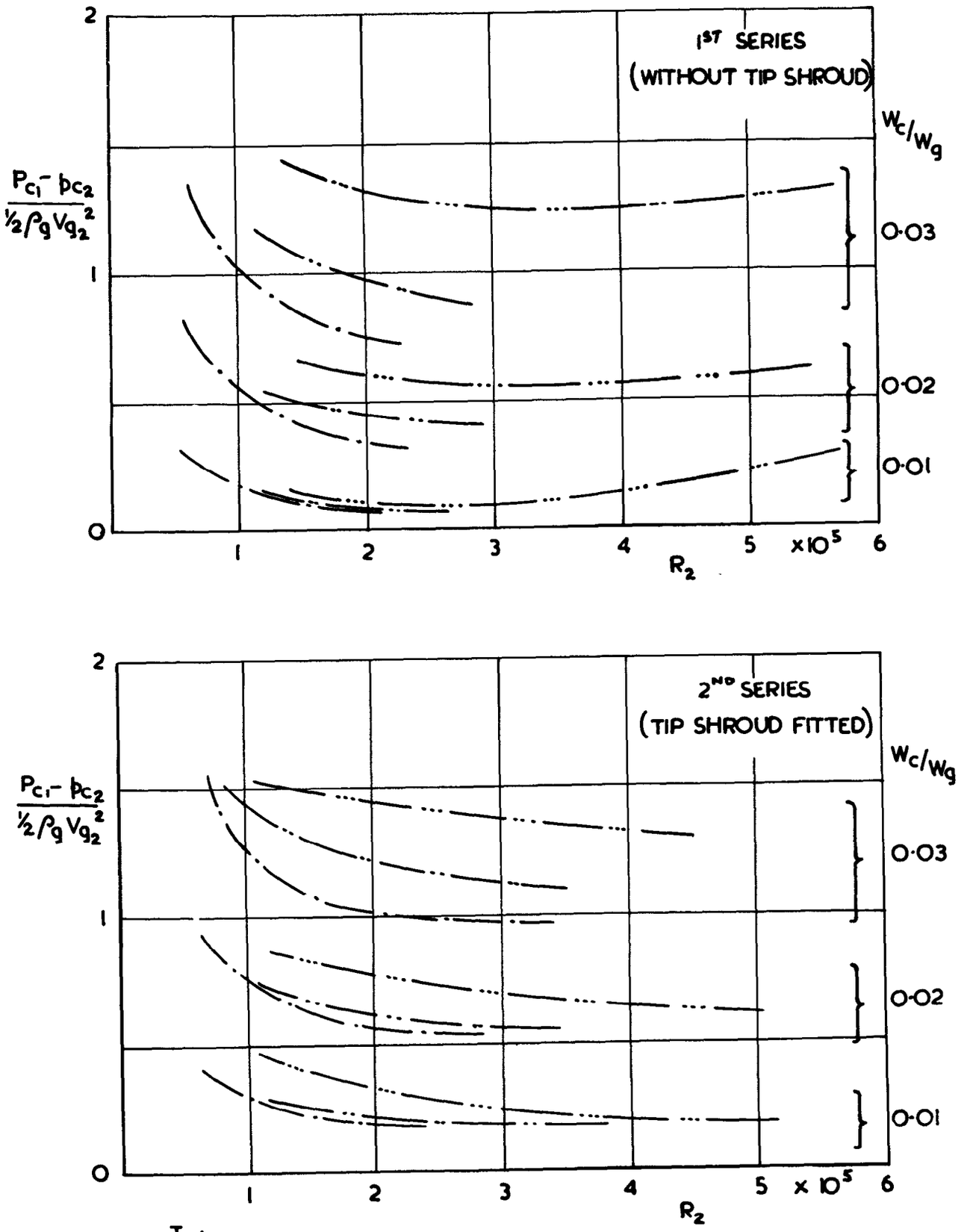

Z 1881/13

COOLANT PRESSURE DROP

FIG.15.

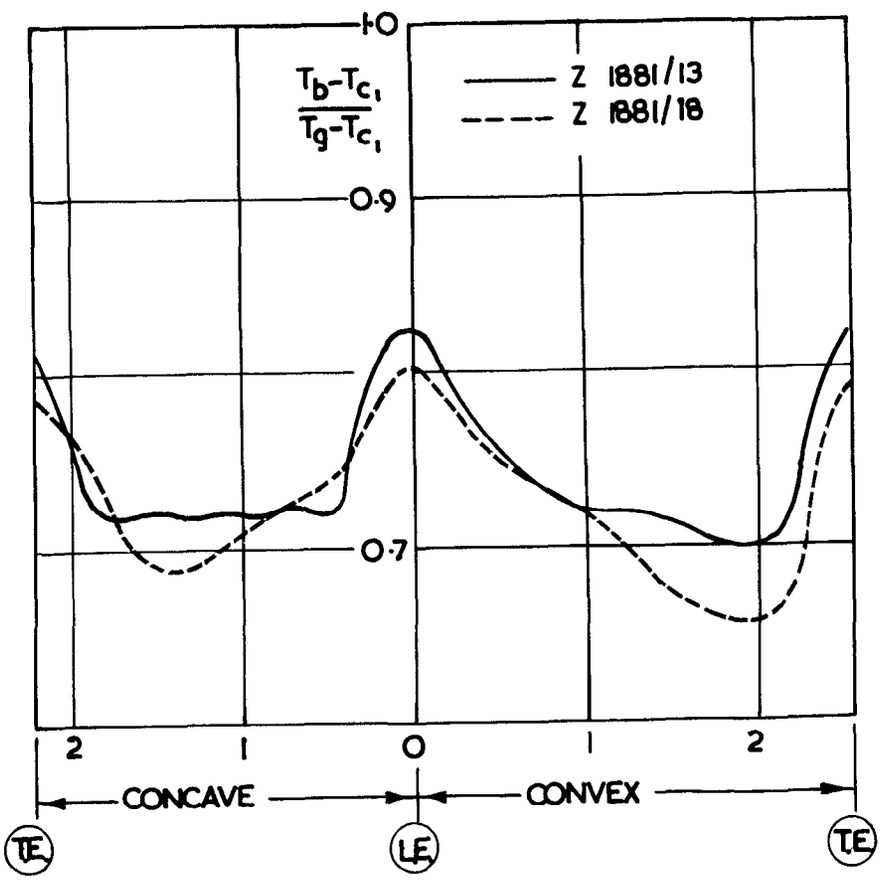

$R_2 \triangleq 2\times10^5$

$T_g/T_{c_1} \triangleq 2$

$W_c/W_g = 0{\cdot}01$

MIDSPAN

BOTH PROFILES TEMPERATURE DISTRIBUTIONS
AT $W_c/W_g = 0{\cdot}01$

FIG. 16.

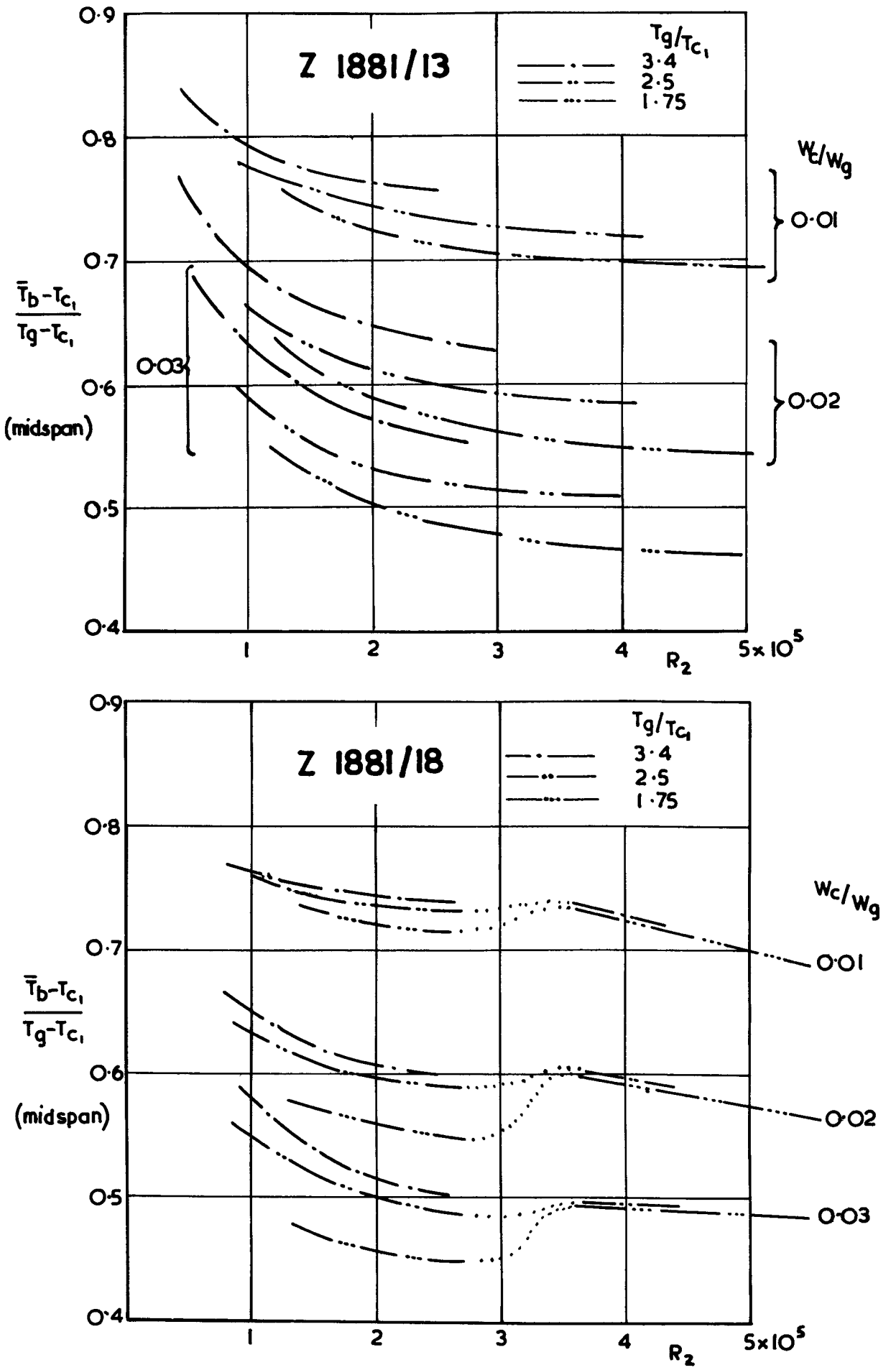

BOTH PROFILES AVERAGE PROFILE SURFACE TEMPERATURE AT MIDSPAN

FIG. 17.

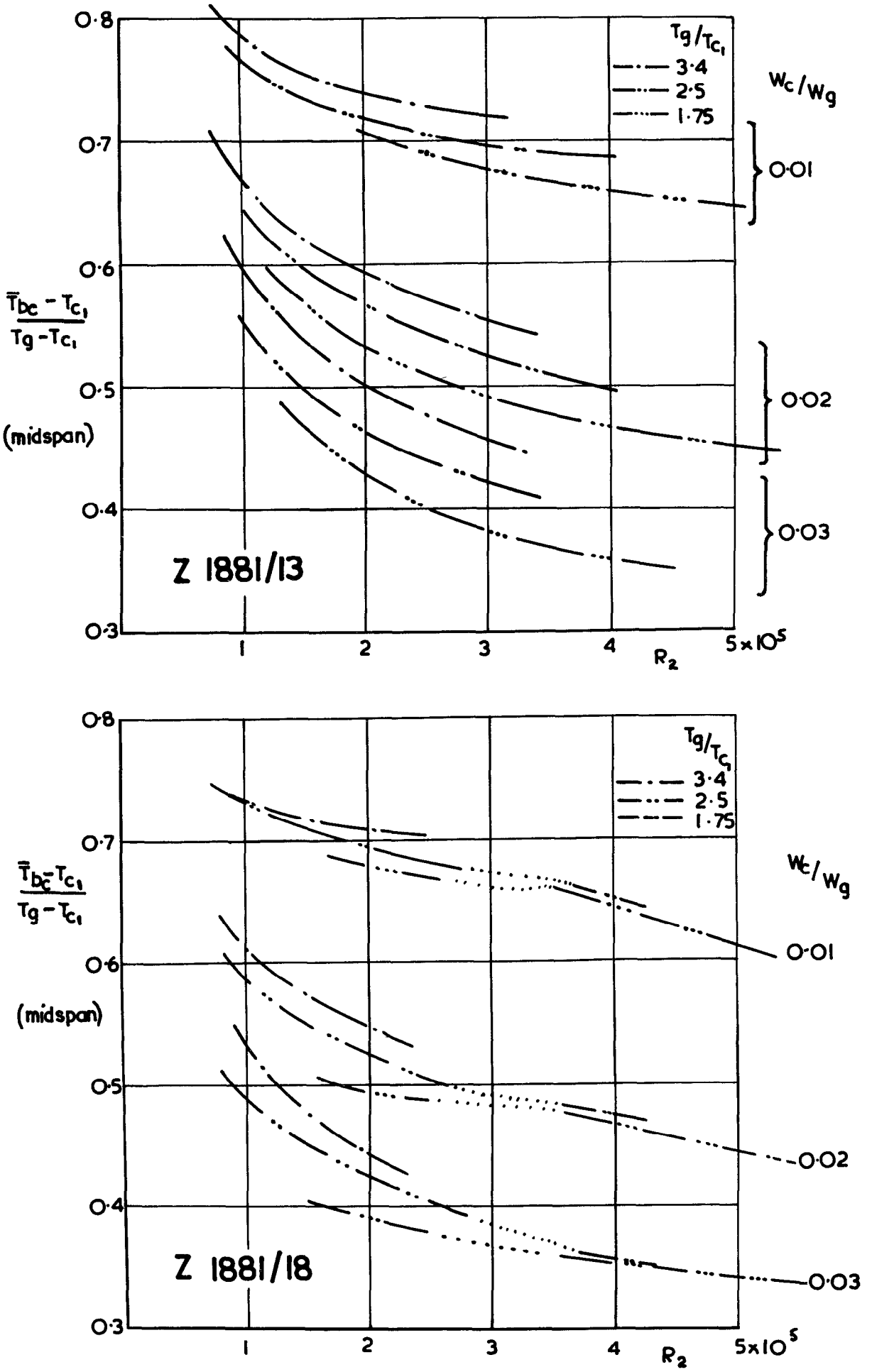

BOTH PROFILES MIDSPAN CORE TEMPERATURE

FIG. 18.

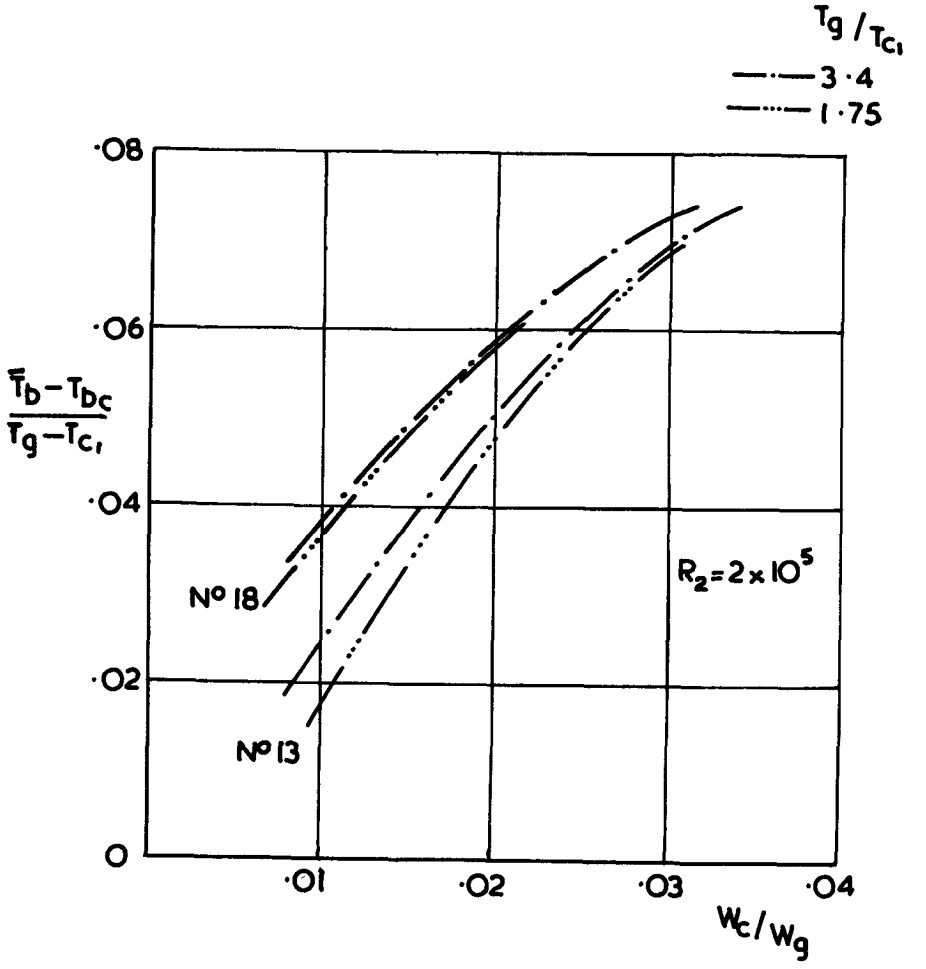

BOTH PROFILES CORE INSULATION EFFECT

FIG. 19

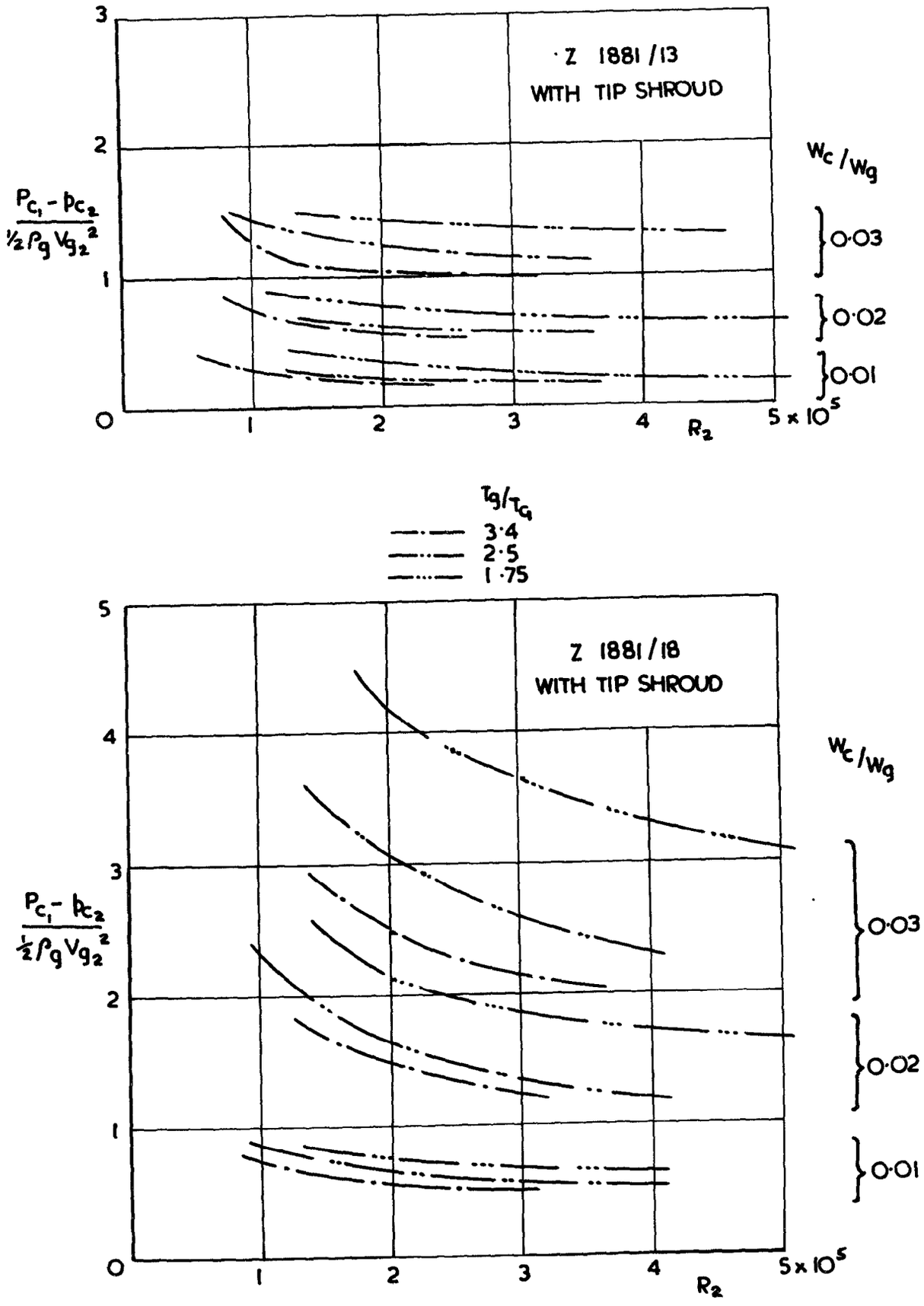

BOTH PROFILES COOLANT PRESSURE DROP

FIG. 20.

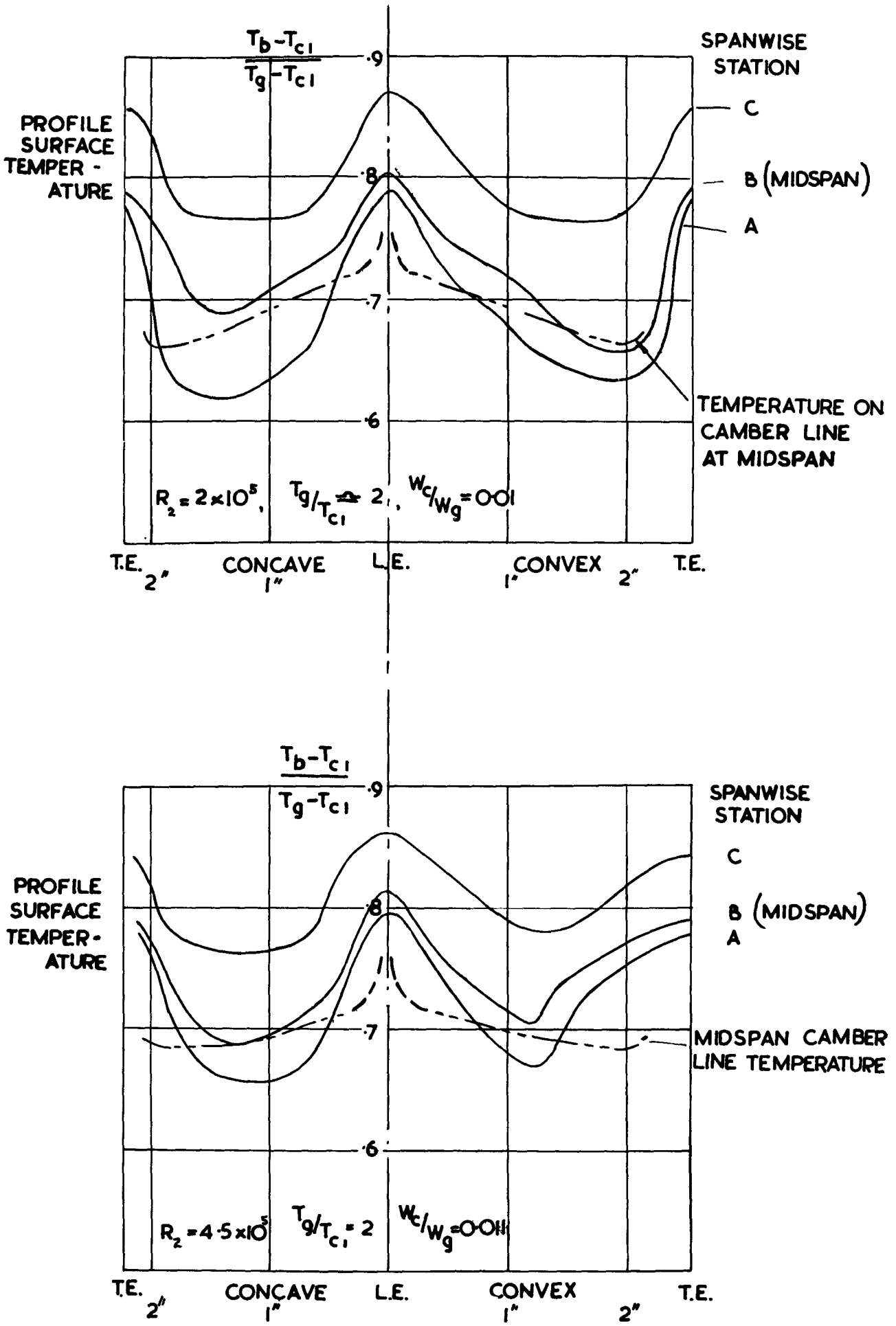

Z 1881/18

TEMPERATURE DISTRIBUTIONS AT VARIOUS STATIONS

FIG.21.

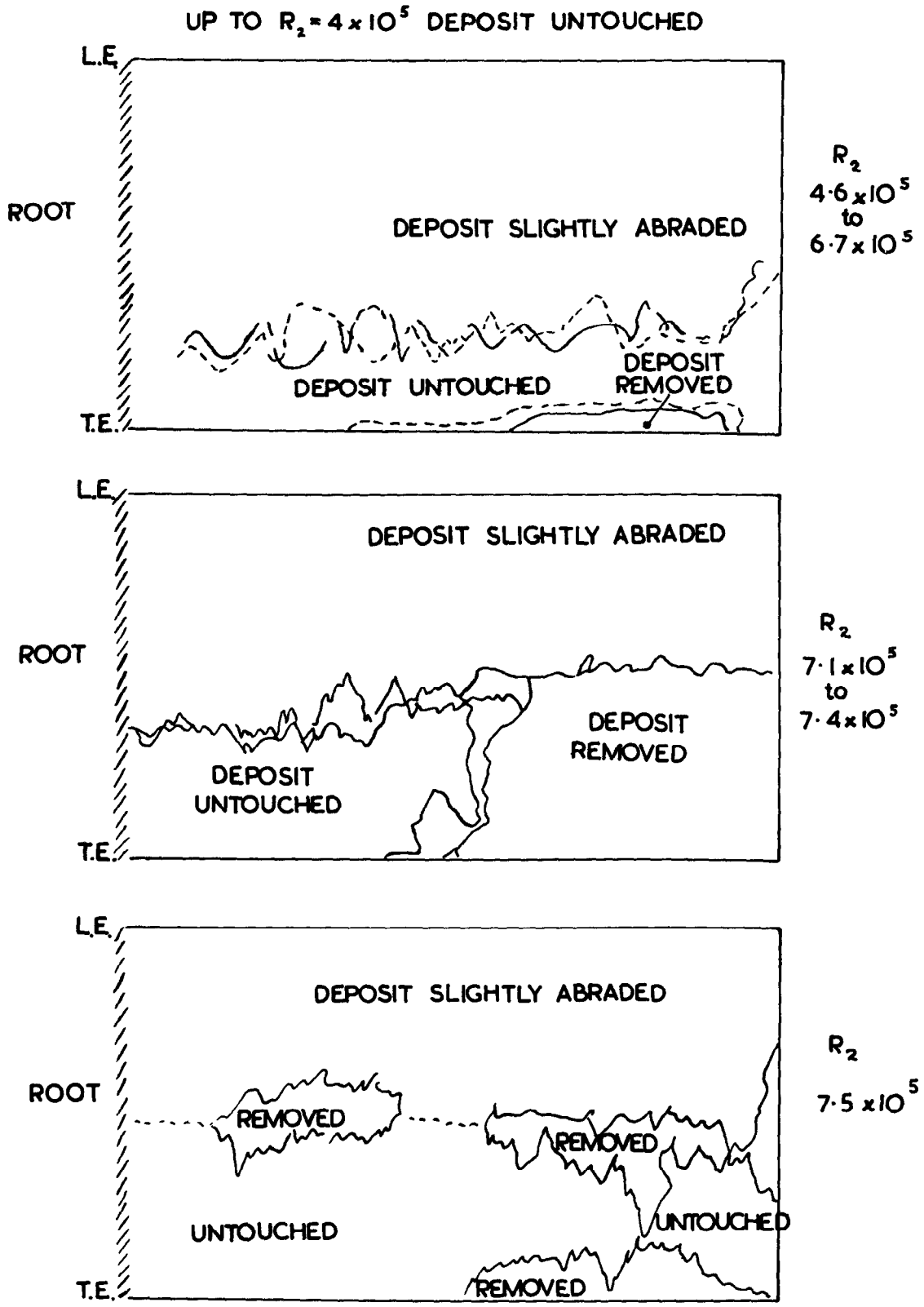

Z 1881/18

LAMP BLACK TRACES AT $T_g = 300°K$

(CONVEX SIDE)

C.P. No. 495
(20,470)
A.R.C. Technical Report

Printed and published by
HER MAJESTY'S STATIONERY OFFICE

To be purchased from
York House, Kingsway, London w.c.2
423 Oxford Street, London w.1
13A Castle Street, Edinburgh 2
109 St. Mary Street, Cardiff
39 King Street, Manchester 2
Tower Lane, Bristol 1
2 Edmund Street, Birmingham 3
80 Chichester Street, Belfast 1
or through any bookseller

Printed in England

S.O. Code No. 23-9011-95

C.P. No. 495